

Dear Erin Pettit,

Thank you very much for your valuable comments. We appreciate your constructive feedback, which helped to enhance the quality of our manuscript tc-2020-133 entitled "Crystallographic analysis of temperate ice on Rhonegletscher, Swiss Alps".

We have considered your suggestions for grammar and writing style and have provided a point-by-point response to your review comments.

If there are further questions, we are happy to answer them and look forward to hearing back from you regarding your decision.

Kind regards,

Sebastian Hellmann and the co-authors.

## **General comments**

*This paper provides a careful analysis of the measured fabric in the central part of a Rhonegletscher, in the ablation area through ice cores (not quite to bedrock).*

*The authors did a really thorough and rigorous analysis of the fabric using multiple thin sections in 3 orientations. The most well analyzed core I have seen for a temperate glacier, I appreciated the thoroughness, as it was necessary because of the dominance by large grains and a grain size distribution that is far from normal. This paper in some form should be published because of the beautiful data set.*

*While the data analysis is done really well, the interpretation in terms of stress state is not as thorough and rigorous. Their qualitative interpretation of the stress state and its relation to fabric and recrystallization processes is confusing and in a few places incorrect. The paper would benefit from a summary of the key states of stress, key metamorphic processes, citing the original research (going beyond Cuffey and Paterson and the Faria reviews). As a reader, if I am to trust their interpretation of the fabric, I need to trust that they understand the underlying physics. At this point, the physics description is still lacking. It is imperative that the interpretation of the fabric in terms of the stresses be written with the same care and rigor that that fabric was measured.*

*First, it would be helpful to clarify when deviatoric stress is being used versus total stress. Deviatoric stress controls most of the deformation and pressure plays a minor, if any, role in deformation, therefore describe the deviatoric stress states rather than "absolute" stress and "overburden." For example, the authors suggest that there is less deformation in the surface layers because the "absolute" stress there is low, but this is not the case - the vertical compressive deviatoric stress is not necessarily smaller at the surface, it is typically about the same - it is only the pressure term in the total stress that is smaller at the surface and pressure does not drive fabric (only gradients in pressure or overburden can drive flow).*

*I would suggest that they re-write the description of the stress state in terms of more formal tensor components, and more specific (and correct) wording. And please be explicit about what is behavior linked to stress and what is behavior linked to strain rate (and discuss with respect to the statement that strain rate ultimately drives fabric development not stress).*

*In terms of writing, there are numerous run-on sentences, imprecise wording, and extensive use of passive voice, all of which slows down the reader. I provide examples of a few of these (but not all of them) below, I encourage the authors to edit carefully for these three writing issues.*

We will check for any passive structures and run-on sentences and appreciate your particular recommendations below. In the revised version, we introduce a subsection about the physical details. We also show the deviatoric stresses for each depth in a separate table and use the particular values for an improved discussion. Of course, the overburden pressure is not responsible for deformation of the ice. We have rectified this blunder.

## **Specific suggestions**

*Line 1 Abstract - the first line of the abstract should offer some kind of bigger picture motivation, something to entice readers beyond those already rheology and fabric "geeks" - this is a neat paper with respect to the unique measurements and it would nice for the broader glaciology community to read it.*

We added a more general introductory sentence:

The crystal orientation fabrics (COF) provide key information about the mechanics of glacier flow as its development is driven by a combination of stresses, strain and recrystallisation. Detailed information of COF can be considered to improve specific parameters for glacier modelling.

*Line 20: delete "to that" - not necessary*

Removed

*Line 23: delete "do"*

Removed

*Line 24: Faria offered great reviews in his 2014 papers, but be careful citing those*

*papers when there are better papers that are more directly or more originally related*

*to the statement. Here by citing Faria, it implies that that paper was the first to discover that COF evolves in a glacier. Provide more direct/original citations please (or be explicit that you are citing Faria as a review article).*

We added the original work:

The stresses and strains occurring within the ice mass not only cause glacier flow, but also induce the development of a characteristic COF and microstructural anisotropy (Gow and Williamson, 1976; Herron and Langway, 1982; Alley et al., 1995, 1997) and summarised in Faria et al. (2014a).

*Line 30: delete "quickly" unless you want to provide the timescale that quickly is indicative of (words like quickly, clearly, mostly, etc don't add any information and can lead to confusion).*

Removed, we revised this sentence according to the first reviewer's comment.

*Line 53 - run-on sentence, breakup into two or three.*

We changed it as follows:

To date, ice core drilling and preparation of thin sections is still a time-consuming process. Only a few discrete measurements are possible within a reasonable amount of time. Nonetheless, the technique for analysing COF has developed extensively, for example, by using image analysis software and powerful

computing resources (Wilson et al., 2003; Peternell et al., 2009; Wilson and Peternell, 2011; Eichler, 2013).

*Lines 74-78 - lots of passive voice here, rewrite*

We changed this to a more active style:

As the ice is just at the pressure melting point, we used a thermal drilling technique (Schwikowski et al., 2014). Although hot-water drillings, performed in the vicinity of the ice core location, showed a mean ice thickness of 110 m, we stopped drilling at 80 m, when hitting some gravel. This gravel blocked the cutter head. We retrieved an 80 m long ice core, with a gap between 46 and 50 m due to technical issues.

*Line 78 - I'm still a little confused how you knew the orientation, did the drill head not spin on the cable as it was lowered or raised?*

Indeed, the core barrel and drill head could rotate, but a magnetometer was integrated into this core barrel. After each drilling we turned this core barrel until reaching the orientation at beginning. Then the core segment was retrieved and its orientation was marked with a knife. Afterwards we tried to attach the segment to the previous one. If this was possible we added a notch with a soldering iron on both segments. However, if this was not possible, we opened up the notch of the knife. Later, we could retrieve the orientation of the core barrel during the drilling process. Assuming that the core segment was not rotating within the core barrel (e.g. due to sudden shocks which we avoided by a decent winch speed), we could retrieve the actual core orientation.

The data also reveal that there is no 360°-spinning around the cable (just slight movements). The water-filled borehole damped any rotation of the core barrel.

*Figure 2/3: I like the diagram in figure 3, but why not just calculate the bulk surface*

*strain rate components from these measurements instead of the figure 3 plot.*

We actually calculate the strain rates as constraint for our model. We will add this information and discuss whether it could replace Fig 3 (or if we keep both as the figure emphasises the smooth decrease in flow speed along ice flow).

*Figure 2/3 - Did you measure the emergence velocity? I would expect emergence, and this will affect the stress state.*

We did not measure this value at this position. However, a reference station about 50 m away from the boreholes shows an emergence of 1.5-2 m a<sup>-1</sup>.

*Line 89 - This paragraph seems to shift to modeling methods, from drilling methods.*

*While it mostly reads ok, perhaps make this a different section? Especially since the section is titled "field site and data acquisition" I also think one paragraph describing*

*the model is a bit thin. If you are actually using the model to interpret your data, please describe it more rigorously and explain the weaknesses with the model output - how much do you trust the modeled principal strain rates and directions? Given that you just assumed a rate factor from another glacier and tuned the sliding to fit this glacier site? Did you conduct a sensitivity study to assess the impact of your parameter selection on the stress and strain rate output from the model? Given that the model inputs are approximate, I'm not entirely sure that the model provides any better qualitative assessment of the expected principal stresses and strain rates than a simpler flow band description explained with clear assumptions.*

We improved the modelling description and moved it to a new section (see substantial changes).

According to your questions: As you point out in your comment for line 97, the model is only used to constrain our interpretation. However, we could have used a flow band description or our borehole data to interpret. The main task behind employing the model is to get some quantitative values rather than just speculating qualitatively about different stresses (namely compressional in-flow and shear stress). The most important weakness is that we use the stress information of a single point to explain the stress conditions for a certain area of the glacier. Local stress effects cannot be captured by such a model. Furthermore, we also do not have reliable bed velocities and we have to admit that the model is only constrained by surface velocity and ice thickness information. To overcome these weaknesses, we will consider strain rates derived from our borehole experiments (Table 3).

*Line 91 - delete "simply"; say "steady state" model or something like that.*

We revised the whole paragraph and removed it.

*Line 97 - I realize that the model is not intended to be a perfect match, but tuning the model to only one surface velocity is limiting. But I think that's ok, if you are mostly going for the style of stresses and not the real magnitudes (but see my comment above about just using a simpler flow band description because models like this not tuned well can induce complexities that might be interpreted as real). Importantly, the stress distribution with depth at the site of the borehole is highly dependent on the sliding coefficient. When you use these results to interpret the data, please discuss this with respect to the limitations of the model (see my comment above about the*

*vertical distribution of stresses). Oh - and what was used for accumulation/ablation rates? The vertical strain rate at the core site will depend on the ablation rate. Did you measure the vertical velocity at the surface?*

We do not model a time-transient evolution but only calculate the stress field for the actual geometry. Therefore, we did not consider the accumulation and ablation rates. The limitation is that the model only provide stresses and not strain rates or directions. We can calculate strain rates with Glen's flow law. Please regard the model as constraining information for the interpretation. We do not intend to setup a perfect model that describes the ice flow and stress + strain rates. This needs additional measurements and is beyond the scope of this work. In the revised interpretation, we also consider strain rates derived from the borehole data.

*Line 123 - delete "as discussed later" and "important" - they don't provide any useful information here.*

Changed.

*Figure 5 - nice figure, I am interested in the other 2 eigenvectors - are they equal? Also, please provide some examples of the size distribution (histogram? or statistical distribution curve? You have some statistics in table 2, at a minimum, provide the median. But I would suggest putting the size distribution for each depth in the supplementary information. Put a reference in Figure 2 caption to Table 2 and the supplementary information for the size distribution.*

We add the other two eigenvectors (Fig 5), symbol size decreases accordingly. The eigenvalues are not 100% equal but both around 0.10-0.31 (we added the particular ranges in the text, line 181). Usually the second eigenvector is laying in the vertical plane of the diamond shape pattern.

We also add the number of grains for 6 grain size classes (<1/1-5/5-20/20-100/100-500/>500 mm<sup>2</sup>) to Table 2 and show a histogram for a selected depth and put the others to the supplement. We will use this additional figure in our interpretation as the small grains (<1mm<sup>2</sup>) clearly emphasis one of the four clusters. This provides some evidence that recently recrystallized grains in the deeper and intermediate parts of the glacier prefer one of the clusters rather than equally distribute to all four clusters.

*Line 166: "oriented in the direction of glacier flow - just be more specific with wording here. The c-axes points within xxdeg of the flow direction (155deg).*

We changed it as follows:

... the azimuth of the maximum eigenvectors ( $147^{\circ} \pm 31^{\circ}$ ) is aligned with the direction of the glacier's ice flow ( $155^{\circ} \pm 10^{\circ}$ , cf. Figs. 1, 2).

*Line 180 - I think this section would be best started with an overview of the deviatoric stress state (if it isn't already in the background), as measured from the surface stakes and as inferred from the model, in terms of the stress tensors and principal directions.*

See substantial changes: we introduce the interpretation with such an overview in lines 200-218. In addition, we add tables with the respective components of stress and strain rate tensor.

*Line 181 - This first sentence doesn't add anything and isn't necessary and is subjective. Just cut it.*

Removed.

*Line 192 - see my note from line 180. It is difficult for me to separate the effect of the longitudinal compression alone - I'd rather see a description of the full deviatoric stress state as a function of depth and then look at what components are doing most of the work. Also, there are two horizontal stresses ( $\sigma_{xx}$  and  $\sigma_{yy}$ ) better to describe these as longitudinal and transverse.*

See substantial changes: we introduce the interpretation with such an overview in lines 200-218. In addition, we add tables 2+3 with the respective components of stress and strain rate tensor.

We also considered your recommendation to distinguish between the dominant longitudinal and the transversal stress.

*Line 198-202 - Misorientation is most likely, is there a need to go into complex (and incorrect) explanation about surface stress? See my comment above that the "absolute stress" doesn't affect the fabric, only the deviatoric stresses do. This is a really fundamental point, please interpret your fabric in terms of deviatoric stresses.*

We removed this immature argumentation.

*Line 211 - I'm not sure I understand this, overburden doesn't generate anything, only gradients in overburden (even better to use formal deviatoric stress terminology).*

We completely revised this paragraph (see substantial changes). The parts where we referred to overburden pressure have been removed. Instead, we introduce our interpretation with an explanation that it is the deviatoric stress driving the deformation.

*Line 228. I think the author is referring to recrystallization when they say "these processes" - please note that it is not true that they were "just attributed to temperature" - cumulative strain has always been known to be a key part of the process. Please cite earlier work - maybe back from the 70s or 80s on this rather than suggest that this is new knowledge?*

Here (and more in detail in the discussion), we introduce the concept of Faria et al. and also show, where their concept differs from previous literature (see substantial changes). Faria clearly state that the tripartite paradigm is wrong and our interpretation is based on their assumptions (which has been proven by other authors in the last years).

They particularly distinguished between strain-induced boundary migration with new grains (SIBM-N) and strain-induced boundary migration with keeping the old grains (SIBM-O).

*Line 233 Because normal and shear stresses are the two types of stresses, then the statement that a combination of normal and shear must have been involved to create the fabric is minimally useful. Please provide more specific description.*

We completely removed this immature part. Instead we refer more to the recrystallization processes to describe the diamond shape pattern.

*Line 239 what does it mean for a tensor to provide "hints" (that seems to me like an anthropomorphism)?*

This line has been removed. See comments to Line 233 and substantial changes.

*Line 239/240 Do you mean that this site is not 100% sliding? That's the only way to avoid borehole shearing. It seems like the model set up already defined a limited amount of sliding, there must be some non-zero component of tau xz. So that was an input to the model, not an output.*

Our model assumes basal sliding (parameter  $c > 0$ ) and we removed this line during our revision.

However, we also considered no basal sliding in our model for a sensitivity analysis. This would lead to giant rate factors which are unrealistic. Therefore, basal sliding is, indeed, a prerequisite.

*Line 241 A parabola is typically for an  $x^2$  relationship, that is not the case for the curve resulting from Glen's flow law.*

It is a hyperbolic curvature.

*Line 243 - how long ago was "recently" can you provide estimates for the timescale of the last significant change in stress state and express that timescale as a percent strain the crystal experiences?*

"Recently" must be within the last four decades as the ice flow direction changed about 1000 m up-glacier and our pattern is in good agreement with the current flow direction. The strain % is difficult to assess as we do not have information about the surface velocities in that area further up-glacier.

*Line 244 - I think the authors mean "latter" not "later"*

Changed.

*Line 244 - I'm not quite sure why a mean grain size reduction would necessarily*

*occur after a change in flow direction, unless you are suggesting that the change in direction is triggering specific recrystallization (migration or rotation). I am also not sure I understand the citation to Faria here, as recrystallization has been described in many papers before. Perhaps you can be more specific about what Faria contributed that is specific to this analysis? And please more carefully cite the statements here (alternatively, if you write an overview of the stress state and metamorphism of the crystals in the beginning that describes and cites each process as background and properly cited, you can avoid having to add too many citations in this discussion section.*

As described in our answer to line 228, Faria was (to our knowledge) the first, who distinguished between SIBM-O and SIBM-N. Others only referred to dynamic and rotational recrystallization (RRX). This distinction is particularly important for observed grain-size changes at high temperatures as in our case. That even leads to a new process understanding, e.g. Steinbach et al (2017) in *Frontiers in Earth Science*, Vol 5.

We include a paragraph in the discussion and describe in detail, how the findings of Faria et al. differ from previous studies (see substantial changes).

*Line 256 I really like the images of the bubbles and the grain boundaries - it does show fast grain boundary migration and active interaction between bubbles and boundary movement. How do you know it was a "complete" recrystallization?*

We actually do not need this Figure anymore and do not use the observations in our revised version.

*Line 258 The image of bubbly and bubble free ice brings up a question I have as to whether there are signs of refrozen water in these thin sections. Water filled crevasses refreeze with a different microstructure that is typically bubble-free or with patterns of bubbles and distinctly different crystals. Some of the small grain "fracture" noted in the paper also might be a post-depositional process. Perhaps it is ok to include these in your analyses, as the same crystal evolution processes are happening, but it might be useful to discuss the ice from snow compaction versus any refrozen water and how that might influence the fabric and grain size distribution (and bubble)*

We have seen those fracture traces in two depths (22+45 m). We also analysed these fracture grains separately and can provide information about their orientation. Some of them are perfectly aligned with the surrounding large grains (especially if the fracture is thin). Others (if not a fracture but rather a patch of small grains) show a girdle structure. This girdle is aligned with the glacier flow (extension in transverse direction). We could exclude these grains from our analysis. This would emphasise the diamond pattern in 22 and 45 m.

*Line 265 - again, I believe you mean to use the word latter.*

Changed.

*Line 265 - please define "fast" - fast compared to what? How fast is fast?*

In the revised version, we do not refer to "fast" recrystallization anymore. However, we included a sentence that the orientation of the patter is in

alignment with the current glacier flow. The glacier has flown in this direction for about 30-40 years.

*Line 273 - delete "as employed in our study?"*

Changed.

*Line 278 - again, Faria is not the first one to say that temperature is not the only driving process behind boundary migration recrystallization.*

This is true, but to our knowledge, Faria is the first one who distinguished between SIBM-N and SIBM-O which assumes a reorientation of old grains (SIBM-O) or a complete creation of small new grains (SIBM-N). According to his model and considering our strain rates and temperatures we have SIBM-N conditions here. This is the difference to earlier studies.

We rephrased according to the calculated strain rates from borehole measurements.

See substantial changes for more details.

*Line 280 - be careful using such a strong word as "only" - also, this is a long run-on sentence and would be better to be split up and explained in more specific wording.*

Thank you, we rewrote this long sentence and consider, that we do not have 100% evidence for our argumentation and thus "only" is omitted here.

*Line 280-295 - These sentences don't actually explain how the diamond shape forms, just that it happens at high strain rates in certain orientation of stress. Rewrite this to explain the underlying physical process, if possible. If not possible to explain the physics, then explain this as being associated with specific conditions, with physics still to be determined.*

We cannot explain the exact physical processes but we rewrite our suggestions that may be responsible for the diamond pattern.

*Line 290-291 - The word "only" is too strong, this sentence seems to be a hypothesis you are trying to suggest that your data support (but I don't know what the "certain strain rate" is).*

Here we need to be more conclusive and argue with the actual values of strain rate.

*Line 293 - "the absolute strain rate... is expected to be" - please clarify which components of the strain rate tensor you are referring to, or if you mean the effective strain rate (tensor invariant). There is very little discussion of inherited fabric in this paper, How does inherited fabric affect the deeper layers (I don't agree that the surface is necessarily inherited because of any less strain rate at the surface - the only component of the strain rate tensor that is smaller at the surface is the simple shear parallel to the bed).*

This paragraph was revised. The strain rate and also the deviatoric stress is not smaller at the surface compared to other depth (Table 2).

*Line 310 - how do you judge "good agreement"?*

We wanted to point out that the stress conditions in these laboratory experiments are in a similar range as we find them in the glacier. During our revision, we rephrased this part.

*Line 317 - "clearly" is not a helpful word - at this point, I am a bit bogged down in generalities and imprecise wording in the fabric and stress/strain relationship, that I am struggling to judge for myself what the source of the 4 maxima are.*

We avoid these words in the revised version.

*Line 335 - I do believe twinning has been observed use EBSD (such as Obbard's work on the Fremont glacier and/or at Siple Dome), I can't remember which one she noted the a-axis alignment that would suggest twinning.*

Up to date, we could not find the respective part in the papers of R.W Obbard. However, her work is worth to consider as it clearly points out the ambiguities of our technique (analysing the c-axis without the a-axes information).

*Line 340 - This statement isn't correct, at least the way I am understanding it (increasing overburden/pressure). Please describe the fabric in terms of deviatoric stress tensor as a function of depth, and, in addition, explain more clearly why 4 single maxima are created rather than a girdle, I think you tried to explain this, but it didn't come through very clearly.*

Indeed, this needed a revision. The overburden pressure is hydrostatic and not responsible for strain rates that drive c-axis developments. We removed this argumentation and included a paragraph in which we describe the physics (i.e. deviatoric stresses) leading to deformation and COF changes.

*Line 346 - yes, in terms of "comprehensive" analysis of the thin sections measurements - this paper is awesome. In terms of interpretation based on stress state, this paper needs work. There have been some other work on temperate glaciers (including some ongoing work on a glacier in Alaska I think - by Gerbi and others? I'm not sure the status of their publications).*

We agree that we have to revise the interpretation part and added a couple of additional details about the stress state in the glacier as derived from the model and further provided information about the strain rates from in situ measurements. These data should simplify the interpretation and allow a better access to the information provided in our paper.

We also figured out that there are a couple of presentations from Gerbi at AGU. However, there seems to be no field data published yet.

Dear Peter Hudleston,

We appreciate your constructive and valuable comments to our manuscript tc-2020-133 entitled "Crystallographic analysis of temperate ice on Rhonegletscher, Swiss Alps".

We have considered your typographic recommendations and have provided a point-by-point response to your review comments.

If there are further questions, we are happy to answer them and look forward to hearing back from you regarding your decision.

Kind regards,

Sebastian Hellmann and the co-authors.

## **General comments**

*This paper provides a detailed description and analysis of the crystallographic fabric of ice taken from a core from the surface to bedrock in the central part of the ablation zone of a temperate valley glacier. It finds that multimaxima fabrics of the type commonly found in most valley glaciers, usually just from near-surface samples, occur at all depths within the glacier, with some systematic changes with depth in orientation of the clusters that constitute the fabric. This is a new finding and deserves to be published on this basis alone. The paper then, importantly, relates the fabric to the stress field derived from numerical modeling and finds a direct relationship between the orientation of the fabric and orientation of the modeled principal stresses. This leads to a possible explanation of these four maxima fabrics. I question parts of the interpretation and don't believe these fabrics are yet fully explained, as discussed in the specific comments below, keyed to lines in the text. I have also corrected a few typographical errors and made some suggestions for language usage.*

We considered the typographic recommendations in the most recent version. Based on the reviewer comments, we revised the modelling part and recalculate the values from the model. The new results slightly change our interpretation and also fit better to your explanations. We are going to add the actually derived values for the stress components to the interpretation part to improve the argumentation. Furthermore, we will remove Fig. 9 as it may not fit to the improved results anymore.

The recommendations about grammar and language, especially in the first sections are already included (comments like "changed")

### **Specific suggestions:**

*Line 9-10. The language here doesn't clearly describe the observed relations, since there are four azimuths and colatitudes that define the fabric and three principal stress directions. It is the centroid of the fabric and the maximum principal stress direction that nearly coincide in orientation.*

We changed this sentence:

The centroid of the four-maxima patterns of the individual core samples and the coinciding maximum eigenvector align with the compressive stress directions obtained from numerical modelling.

*Line 31. The stress and kinematic conditions in valley glaciers are more complex than just combinations of simple and pure shear.*

Changed to:

In contrast, for ice samples from temperate glaciers, the deformation is dominated by a series of interfering and variable compressional, extensional, and shear stress conditions along the flow in the valley.

*Line 94. Although the details of the numerical model need not be given here, the basic form of the flow law should be given, since the value of the flow law parameter  $A$  is defined. The value of the power law exponent,  $n$ , in the flow law should also be noted.*

See our remarks for substantial changes. We added a new section and provide the basic equations for ice flow and the Weertman's friction law. We also define/describe the respective parameters.

*Line 117. It is not clear what is meant by fractures here, since there are no actual fractures in this core. This needs clarification. What are the physical manifestation of the 'fractures?' They must be defined by some combination and bubble or grain size distribution.*

We changed it to "fracture traces" as recommended in your comment for Line 151. However, in other literature we found the term "fissures". As it seems not to be conclusive, we use both terms.

*Line 135. Surely this is mm<sup>2</sup> not  $\theta$ m<sup>2</sup>*

Indeed, this must be mm<sup>2</sup>, changed.

*Line 151. Here is some information about the fractures. Presumably these patterns are in the form of linear traces in thin section. Following Hambrey I like the term 'fracture traces' for these likely healed fractures.*

We changed it to "fracture traces" as a much better name for these features that could be observed in some core depths. However, they are sometimes called fissures. Therefore, we mention both names.

*Line 157. You use the term centroid here for the maximum eigenvector on these plots, and state that these are equivalent in the caption to Table 1. Yet in Figure 7 the two are represented and plotted as separate entities. The usage needs to be consistent. In this case how is centroid defined?*

We revised the usage of centroid and centre (i.e. midpoint) between the clusters. The midpoint (red dots in Fig. 7) is defined as geometric point between the four maxima (independent of number of grains per cluster). The centroid is affected by the particular distribution of grains and those maxima with a larger grain number attract the centroid. Therefore, midpoint and centroid differ slightly. When calculating the opening angle we considered the midpoint as symmetry point of the multi-maxima pattern.

*Line 173-174. It should be noted that Kamb, Hooke and others have discussed the issue of accounting for complex and branching shapes of large grains when making c-axis plots.*

We added the recommended references and furthermore two papers that also show images for a better visualisation:

Therefore, two-dimensional cuts through large, branched grains may let them appear as several individual grains within the same section. Kamb (1959) and Hooke (1969) have already discussed the statistical relevance of these branched grains. The sketches in Hooke (1980), Fig. 6 and more recently in Monz (2020), Fig. 3, further illustrate this issue that could result in over-represented clusters in the superimposed stereo plots from the different sub-samples.

*Fig. 6. The caption could be shortened by stating that the annotation is as in Fig. 5*

Changed.

*Line 192. The c-axis fabric has orthorhombic (and perhaps close to axial) symmetry, but is this also true of the stresses? What about the other two principal stresses. Are they consistent with plane strain or plane stress, as appears to be assumed in Fig. 9? Are the principal stresses and strain rates in this section of the glacier near the surface parallel to the flow direction ( $\sigma_1$ ), vertical ( $\sigma_3$ ) and horizontal ( $\sigma_2$ ), with the lateral strain rate close to zero, as one would expect for a valley of constant width. One would expect the maximum principal stress to become inclined deeper into the ice as shear stress parallel to the base increases, which the modeled stress shows a tendency to do.*

We added the requested components to Figs 5 (eigenvectors) + 7 (stresses). The eigenvalues are named with  $\lambda_1$  -  $\lambda_3$  and the stress axes with  $\sigma_1$  to  $\sigma_3$  in descending order. The symbol size decreases respectively in both Figures.

We assume, that the eigenvectors are aligned with the strain rates (i.e. deformation). Due to the non-coaxial relation for simple shear, the eigenvectors could differ from the stress principal axes by up to 45°. Under this assumption,

the largest eigenvector in 79 m is perfectly aligned with the strain rate direction for dominating simple shear.

Figure 9 was removed due to speculative parts (see substantial changes).

*Line 200-204. This is a possible explanation, but I prefer the misorientation of the sample as the explanation, which as you state, fits very nicely when a 60° azimuthal 'correction' is made. A preserved fabric from earlier in the flow path is less likely at high temperatures when rapid recrystallization is expected.*

We removed this immature hypothesis, especially as we cannot see a smaller deviatoric stress in the uppermost parts.

*Lines 210-213. With this explanation you would expect  $\sigma_1$  to be vertical to explain the fabric at 79m depth and not as given by the numerical model. Although the vertical normal stress increases with depth, it is the deviatoric stress that controls deformation, not absolute stress values, and this likely does not change greatly with depth. I think the main thing that changes with depth is not the vertical effective compression ( $\sigma_1 - \sigma_{\text{mean}}$ ) but the increasing addition of base parallel shear stress, that in general terms increases linearly with depth.*

Our mistake was to consider a (hydrostatic) overburden pressure. However, this hydrostatic pressure does not contribute to the deviatoric stress that drives the c-axis orientation (via strain rates). We revised this part accordingly. As you say, the c-axis orientation (i.e. the centroid) in the deepest part is in alignment with shear stress: Base-parallel shear stress lead to a base-parallel orientation of the basal planes and thus a more vertical c-axis. The model shows that the shear stress component  $\sigma_{xz}^d$  (which we will add to the results section) is the most dominant stress and the in-flow compressional component  $\sigma_{xx}^d$  is much smaller in this depth (similar to  $\sigma_{yy}^d$ ).

*Line 217. There is almost certainly some dependence of fabric on strain, which may not be great with fast recrystallization.*

We revised the details about recrystallization. Now, we consider, that strain-induced grain boundary migration with nucleation of new grains is the driving force. Then we do not have to assume any "fast" or "complete" recrystallization.

*Line 213-214. In simple shear the directions of principal stress are only aligned with those of principal strain for infinitesimal strains. The divergence grows as strain increases.*

We assume that strain rate (and the strain) and stress direction form an angle of  $\sim 45^\circ$ . Therefore, the principal stress direction (governed by the simple shear component) in the deepest part of  $\sim 48^\circ$  and the actual centroid ( $\sim 2^\circ$ ) would fit under such an assumption. The MM cluster is aligned with the strain rate direction in that depth and not with stress as stress and strain diverge for simple shear.

*Line 238 I don't believe Cuffey and Paterson really explain why there should be*

*four maxima when the stress deviates from unconfined compression. This is more of an observation than an explanation.*

No, they only provide a description and mention different stresses are required for multi-maxima. In the revised version there is no need to cite them. We considered the more specific literature.

*Lines 244-245. This is unclear. A change in direction of glacier flow could be associated with either an increase or decrease in strain rate and thus decrease or increase in recrystallized grain size. Why just a decrease?*

This is correct, it could be an increase as well.

In our detailed description for SIBM-N and SIBM-O we discuss in detail, how the grain size evolves under different conditions.

*Line 251 and Table 2. Table 2 does not really give the grain size distribution, only average numbers of grains and average and maximum size in each sample. It would be useful to know the number of grains in each size category. Also interesting to know if there is any difference between the large and small grains in COF.*

We added a supplementary figure (Fig. 8, revised version) and median and 6 different grain size classes to Table 2 (now Table 4).

*Line 255-266. I'm not sure how much information is given by the air bubbles, except they do provide excellent evidence of active recrystallization by grain boundary migration. Bubbles are found both within grains and along grain boundaries both in temperate ice and in cold ice experiencing dynamic recrystallization, although the recrystallization mechanism may differ.*

As we found a better way to explain the recrystallization processes, we removed this Fig. 8

*Line 269. Hooke and Hudleston were concerned with polar, not temperate ice. The study was made on the Barnes Ice Cap.*

Thank you, again a valuable hint. We will change it:

They were observed in early studies on temperate glaciers (e.g., Rigsby, 1951; Kamb, 1959; Rigsby, 1960), ice capes with ice temperatures above  $-10^{\circ}\text{C}$  (Hooke and Hudleston, 1980), and also in the bottom ice of Byrd Station and Cape Folger in Antarctica (Gow and Williamson, 1976; Thwaites et al., 1984). They are often referred as "diamond-shape" pattern or fabrics.

*Line 276. Whether the multimaxima fabrics are a result of unrepresentative sampling is still arguable in some circumstances, although the case you have here for these being true multimaxima fabrics is a strong one.*

Due to an additional analysis (Fig. 8 new manuscript), we can provide further arguments for the existence of multi-maxima pattern.

*Line 290-291. I think more data is needed to support this conclusion. The cores taken by Tison and Hubbard were in a different regime within the glacier – accumulation zone where perhaps there is longitudinal extension rather than compression, and close to the lateral margin of the glacier rather than in the center. This must lead to a more complex stress regime.*

Actually, some cores were drilled in the ablation zone and in these cores they found multi-maxima at the bottom. However, it is true that they are drilled at the margin and therefore they could significantly differ from our core close to the centre flow line of the glacier. This could complicate a direct comparison.

*Line 298-299. The combination of compression plus simple shear as applied in these experiments makes sense for much of your core, but not for the highest one where the shear component is minimal, nor for the lowest one, where the  $\sigma_1$  direction lies well outside the small-circle girdle of maxima. Some other explanation must hold in these places.*

Our revised interpretation assumes that the multi-maxima pattern clusters around the dominant strain rate direction, which is the one of base-parallel simple shear for this depth. The eigenvector is aligned with the expected strain rate direction (as you also describe). Due to recrystallization, we observe the clustering of four maxima around this axis.

*Line 300-301. I'm not sure if I'm properly interpreting what you are saying here, but the planes of maximum shearing stress in Duval's combined compression-simple shear experiments are not vertical and horizontal in his experiments, but inclined by an amount that depends on the relative amounts of normal compression and simple shear.*

This is exactly, what we wanted to cite here. His experiments show a multi-maximum pattern that is aligned with the compressional axis and two of these maxima are also aligned with the poles of the two shear planes as the angle between the maxima and the principal direction is roughly

*Line 312-316. Both Llorens et al. and Qi et al. are dealing only with simple shear, not with combined compression plus simple shear as in the torsion plus compression experiments. The conditions in the Rhone glacier I imagine change from horizontal compression with minimal base-parallel shear near the surface to horizontal compression combined with increasing base-parallel shear near the base of the glacier. As theory shows, shear stress increases approximately linearly with depth, while longitudinal stress stays approximately constant.*

This part has been removed. We cite Llorens to discuss potential localisation effects. However, Qi et al. are not providing any additional information useful for our interpretation.

*Fig. 9. The stress state shown in Fig. 9 is almost that of simple shear (no base-parallel longitudinal compression) with the shear plane (taken as the glacier bed) horizontal and  $\sigma_1$  inclined at 45° to the shear plane. If it is simple shear, there will be no horizontal compression and thus no shortening in the glacier flow*

*direction, which is incompatible with your data. If horizontal glacier flow-parallel compression is added  $\sigma_1$  will move closer to horizontal than it would be for simple shear alone. This looks like being the case for much of the glacier from the stresses shown in Fig. 7. I would expect the inclination of  $\sigma_1$  to be near zero at the surface and something less than 45° close to bedrock, the amount depending on the amount of horizontal compression. Although not a smooth change, the  $\sigma_1$  directions in Fig. 7 are consistent with this. The plot in Fig. 9 does not correspond to any of the plots in Fig. 7, all of which have  $\sigma_1$  at a shallower inclination than 45° and thus have associated planes of maximum shearing stress that are neither vertical or horizontal, unlike the situation in Fig. 9. The one closest to horizontal thus cannot be considered a plane of simple shear. The 'shear plane' must always be the presumably sub-horizontal glacier bed.*

This Figure cannot hold a substantial revision. Therefore, we removed it and all parts in the text.

*Line 340. I disagree with the statement here (see comments for lines 210-213). Although the absolute value of the vertical normal stress increases with depth, the deviatoric vertical normal stress changes much less. It is the increase in base-parallel shear stress combined with the horizontal compressive stress ( $\sigma_{xx}$  if you like) that causes  $\sigma_1$  to rotate from near horizontal at the surface to inclined at some angle of less than 45° at the base.*

Indeed, the vertical stress  $\sigma_{zz}^d$  is not responsible and actually decreases in our revised model with increasing depth. We will change this conclusion accordingly and agree with your suggestion that the orientation is driven by  $\sigma_{xz}^d$  and  $\sigma_{xx}^d$

*Line 342. The second part (ii) of the explanation for multimaxima fabrics given here makes no sense by itself. All states of stress that are non isotropic involve shear stresses. If the multimaxima fabric depended solely on the state of stress - that is with instantaneous adjustment of the c-axis fabric as the stress field changes - then there should be a constant relationship between the positions of the maxima and the principal stress directions. This clearly is not the case as the relationship in the deepest sample shows. There is, however, as you note, a consistent relationship between the fabric and the  $\sigma_1$  direction through most of the glacier and in all cases, with small deviations, the centroid of the COF fabric and the  $\sigma_1$  direction lie in the vertical plane that contains the flow direction. This is a key relationship that I believe you have only partly explained.*

We also put a larger emphasis on the fact that the general COF pattern is aligned with the flow direction (with an exception in 79 m).

## **Substantial Changes:**

### Introduction:

Here we flipped two paragraphs as it improves the readability of the manuscript. Furthermore we changed the quickly changing simple and pure shear interfering and changing compressional, extensional, and shear stress conditions along the valley in combination with

### Data acquisition:

We moved the modelling part to an individual section and corrected some writing errors.

### Ice flow modelling

We moved the details of the model to a new individual section.

We provide more details and additional basic equations (Glen's flow law and Weertman's friction law) for a better understanding. Furthermore, we got some information about the basal velocities. We used these information to further constrain our model.

We also include details about sensitivity studies and explain more in detail why we use the respective parameters.

### Crystal Orientation Fabric Analysis

We removed the details about the LASM measurements as they are no longer needed (see changes in Discussion).

### Results

We added some more details about the eigenvectors (values and ranges) and a more precise distinction between mid-point and centroid. Furthermore, we considered literature recommendations from the reviewers.

### Interpretation

Here, we added a general description about the stress conditions in the glacier and highlighted the dominant elements of the stress tensor. Furthermore, we calculate the strain rates and provide all modelled stress and strain rate components in tables. The strain rates cannot be derived directly from our model as we ran it in stationary fashion. Therefore, we calculated the strain rates via Glen's flow law.

We described more precisely the correlations between glacier flow and c-axes orientations for the observed azimuthal and co-latitudinal variations.

For this, we used the previously defined deviatoric stress components as references and to enhance the readability.

Especially in subsection 6.3 we removed the imprecise and speculative parts as criticised by both reviewers. Instead, we provide a detailed description about the recrystallization mechanisms that we believe are most important for our observations. Based on this RX-mechanism we provide an interpretation for the formation of the observed multi-maxima.

We also added further details to the results shown in Table 4 (previously Table 2).

These classifications are more useful for our interpretation than the previously employed LASM scans. Therefore, we removed these LASM-scans and the information about them.

### Discussion

In our discussion, we mainly revised the parts about recrystallization and restructured this section. First, we compare our findings with other field studies, then with laboratory experiments and afterwards we describe in detail the recrystallisation. We explain in detail, why we follow the approach of Faria et al (2014) and explain the

difference to previous studies. Based on these findings we discuss the formation of the multi-maxima pattern. We also consider additional hypotheses and mention them in the discussion. However, we removed the speculative part in conjunction with Fig. 9. This part cannot sustain in a thorough review.

### Conclusion

Based on the changes in our discussion, we also rewrote parts of the conclusion. We mainly included the effects of SIBM-N and removed the (obvious and useless) statements that simple shear and compression are the main driving forces.

# Crystallographic analysis of temperate ice on Rhonegletscher, Swiss Alps

Sebastian Hellmann<sup>1,2</sup>, Johanna Kerch<sup>3,\*</sup>, Ilka Weikusat<sup>3,4</sup>, Andreas Bauder<sup>1</sup>, Melchior Grab<sup>1,2</sup>, Guillaume Jouvét<sup>5,6</sup>, Margit Schwikowski<sup>4</sup>, and Hansruedi Maurer<sup>2</sup>

<sup>1</sup>Laboratory of Hydraulics, Hydrology and Glaciology (VAW), ETH Zurich, Zurich, Switzerland

<sup>2</sup>Institute of Geophysics, ETH Zurich, Zurich, Switzerland

<sup>3</sup>Alfred Wegener Institute Helmholtz Centre for Polar and Marine Research, Bremerhaven, Germany

<sup>4</sup>Department of Geosciences, Eberhard Karls University, Tuebingen, Germany

<sup>5</sup>University of Zurich, Department of Geography, Switzerland

<sup>6</sup>ETH Zurich, Autonomous Systems Laboratory, Switzerland

\* now at: GZG Computational Geoscience, Georg-August University, Goettingen

**Correspondence:** Sebastian Hellmann (sebastian.hellmann@erdw.ethz.ch)

**Abstract.** The crystal orientation ~~fabric~~-fabrics (COF) provide key information about the mechanics of glacier flow as its development is driven by a combination of stresses, strain and recrystallisation. Detailed information obtained from COF can improve specific parameters for glacier modelling. The COF was studied at an ice core that was obtained from the temperate Rhonegletscher, located in the Central Swiss Alps. Seven samples, extracted at depths between 2 and 79 m, were analysed with an automatic fabric analyser. The COF analysis revealed conspicuous four-maxima patterns of the c-axis orientations at all depths. Additional data, such as microstructural images, produced during the ice sample preparation process, were considered to interpret these patterns. Furthermore, repeated high-precision Global Navigation Satellite System (GNSS) surveying allowed the local glacier flow direction to be determined. The relative movements of the individual surveying points indicated horizontal compressive stresses parallel to the glacier flow. Finally, numerical modelling of the ice flow permitted ~~to estimate~~-estimation of the local stress distribution. An integrated analysis of all the data sets provided an explanation for the four-maxima patterns observed ~~four-maximum patterns~~ in the COF. The ~~average azimuths and colatitudes of the c-axes~~-centroid of the four-maxima patterns of the individual core samples and the coinciding maximum eigenvector align with the compressive stress directions obtained from numerical modelling. The clustering of the c-axes in four maxima surrounding the predominant compressive stress direction is most likely the result of a fast migration recrystallisation in combination with the presence of significant shear stresses. ~~This interpretation is supported by air bubble analysis of the LASM images.~~ Our results indicate that COF studies, which were so far predominantly performed at cold ice samples from the polar regions, can also provide valuable insights on the stress and strain distribution within temperate glaciers.

## 1 Introduction

Since the second half of the last century, ice cores have been regarded as extremely valuable archives for reconstructing the climate history of the past hundred-thousands of years (Robin et al., 1977; Petit et al., 1999; Thompson et al., 2002). For example,

correlations between ice accumulation, isotopes and dust content have been established, but the deformation of ice layers complicates dating and interpretation of climate records (Jansen et al., 2016). Microstructural analyses have been used to overcome these issues (Faria et al., 2010). In addition ~~to that~~, microstructural investigations ~~are also~~ have also been conducted to reconstruct the ice flow of ice sheets in Greenland and Antarctica as well as in glaciated mountain areas (Russell-Head and Budd, 25 1979; Alley, 1992; Azuma, 1994). For those investigations, the focus has been on the crystallographic orientation of the ice grains. The stresses and strains occurring within the ice mass ~~do~~ not only cause glacier flow, but also induce the development of a characteristic COF and microstructural anisotropy (~~Faria et al., 2014a~~) (Gow and Williamson, 1976; Herron and Langway, 1982; Alley et al. and summarised in Faria et al. (2014a).

During the past decades, COF and texture have been investigated intensively on polar deep ice cores to understand the 30 microstructure of polycrystalline ice in the context of its deformation history (Hooke, 1973; Gow and Williamson, 1976; Thorsteinsson et al., 1997; Patrick et al., 2003; Gow and Meese, 2007; Montagnat et al., 2014; Weikusat et al., 2017). A historical summary of these projects can be found in Faria et al. (2014a). For the selected ice core drilling spots on domes and ridges, vertical compression and horizontal extension within the ice mass have been found to be the dominant driving stress for ice deformation. In contrast, for ice samples from temperate glaciers, the deformation is dominated by a series of ~~quickly changing~~ 35 ~~simple and pure shear~~ interfering and changing compressional, extensional, and shear stress conditions along the valley ~~in combination with~~. Together with a diagenesis, burial, basal sliding, ~~which and potentially partial melting these stress conditions~~ results in a much more complex deformation history (Hambrey and Milnes, 1977). This requires more extensive analyses of COF. ~~First crystallographic investigations have been performed on temperate glaciers already in the 1950's to 1980's, including the detailed investigations of Kamb (1959) and Rigsby (1960), and later extended by Budd (1972), Hambrey and Milnes (1977), Hooke and Hudleston (1978), and Hambrey et al. (1980). A potential problem of temperate glacier crystal analysis is the large grain size and thus limited amount of grains that can be analysed for each sample. This may be the reason, why a surprisingly low number of papers was published on crystal structure of temperate glaciers (e.g. Tison and Hubbard, 2000) during the past years. Furthermore, the majority of the earlier studies mainly analysed samples from the uppermost few meters.~~

The ice of temperate glaciers is comparable with a metamorphic rock close to its melting point (Hambrey and Milnes, 1977) 45 that has been exposed to a long series of deformation processes along the valley. This deformation is caused by various shear and compressional stresses that have been applied to the ice. These stress regimes produce heterogeneously distributed dislocations, which cause dynamic recrystallisation by rearrangement of these dislocations ~~or~~ and by internal strain energy reduction. The resulting recrystallisation processes and the interplay between deformation and recrystallisation in the ice take place even faster as the temperature gets closer to the pressure melting point (Alley, 1988; Weikusat et al., 2009a). As a result, the adaption 50 of the ice crystal structure to new stress conditions is expected to be faster (e.g. Kamb, 1972; Duval, 1979). Additionally, the higher temperatures provide more thermal energy and allow a faster grain growth (Azuma et al., 2012), leading to an interplay between stress and temperature regime (Alley, 1988; Faria et al., 2014b). Therefore, large differences can be observed between cold and temperate ice. One of the most apparent differences is the grain size, which has been found to be a few centimetres in temperate ice (Rigsby, 1960), whereas samples from polar ice usually show grains with a diameter of a few millimetres, except 55 in the deepest parts, where temperatures rise close to the pressure melting point (e.g. Gow and Williamson, 1976; Thwaites

et al., 1984; Kuiper et al., 2019).

~~Although~~ First crystallographic investigations have been performed on temperate glaciers already in the 1950's to 1980's, including the detailed investigations of Kamb (1959) and Rigsby (1960), and later extended by Budd (1972), Hambrey and Milnes (1977), Hooke and Hudleston (1978), and Hambrey et al. (1980). A potential problem of temperate glacier crystal analysis is the large grain size and thus limited amount of grains that can be analysed for each sample. This may be the reason, why a surprisingly low number of papers has been published on crystal structure of temperate glaciers (e.g. Tison and Hubbard, 2000) during the past years. Furthermore, the majority of the earlier studies mainly analysed samples from the uppermost few meters. To date, ice core drilling and preparation of thin sections is still a time-consuming process, and only. Only a few discrete measurements are possible within a reasonable amount of time. Nonetheless, the technique for analysing COF has developed extensively, for example, by using image analysis software and powerful computing resources (Wilson et al., 2003; Peternell et al., 2009; Wilson and Peternell, 2011; Eichler, 2013).

In this study, we analyse ice core samples from a temperate alpine glacier. We describe and compare our findings with studies from the last century and provide a hypothesis for the resulting COF in terms of given stress and temperature conditions. We analyse the stress regime in the vicinity of the ice core, using additional borehole measurements and discuss recrystallisation processes and grain growth in temperate ice. For selected examples we take a closer look at the development of new ice crystals under the current stress regime of the glacier. The microstructural results of this study serve as a basis for geophysical experiments on ice core samples, ~~which will be discussed in an accompanying paper~~, and they can also be compared with results from larger scale geophysical experiments.

## 2 Field Site and Data Acquisition

The field work was carried out on Rhonegletscher, located in the Central Swiss Alps (Fig. 1). This glacier currently covers an area of about 15.5 km<sup>2</sup> and is flowing in a southern direction from 3600 m a.s.l. down to 2200 m a.s.l. It is a medium-sized valley glacier, easily accessible, and therefore investigations ~~were had been~~ carried out already in the last two centuries and continuously since 2006 (Bauder, 2018).

In August 2017, ~~the ice core was drilled~~ we drilled an ice core in the ablation area of the glacier (Fig. 1), approximately 500 m north of its current terminus. Here, the ice was flowing with an average surface velocity of 16.2 m a<sup>-1</sup> in the season 2017/18 according to GNSS measurements. This location was selected, because the glacier surface forms a relatively even plateau with only 5 m elevation change over a distance of 40 m and is free of crevasses. Further up-glacier there is a steep and crevassed area. An analysis of the bedrock with ground-penetrating radar measurements also confirmed a transition from a steep to a more flat zone of the valley (Church et al., 2018) at the ice core location.

As the ice is just at the pressure melting point, we used a thermal drilling technique (Schwikowski et al., 2014) ~~was used~~. Although hot-water drillings, performed in the vicinity of the ice core location, showed a mean ice thickness of 110 m, ~~the drilling was stopped~~ we stopped drilling at 80 m, when hitting some gravel, ~~which~~. This gravel blocked the cutter head. ~~An~~ We retrieved an 80 m long ice core, with a gap between 46 and 50 m due to technical issues, ~~was retrieved~~.

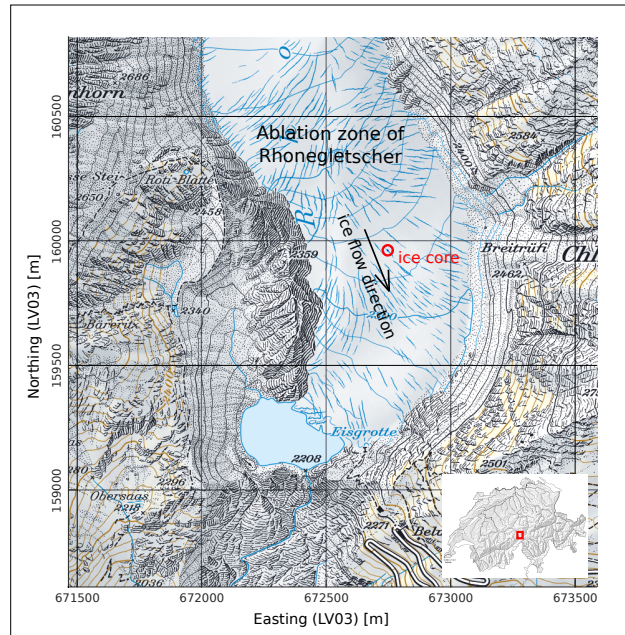


**Figure 1.** Rhonegletscher ablation area, ice core position indicated in red, ice flow direction at ice core location shown by black arrow.

Due to the thermal drilling technique, which did not apply a rotational force onto the ice core segments, an oriented retrieval of the segments was possible. A freshly drilled segment was manually connected to the previous one, which worked out well for most of the segments. Additional measurements of the Earth's magnetic field, while drilling, could be used in some cases to reconstruct the orientation within a range of  $\pm 10^\circ$  when matching of neighbouring segments was not possible.

To complement the results of the ice core analysis, we made use of an array of hot-water-drilled boreholes surrounding the location of the ice core retrieval (Fig. 2). The locations of the borehole collars were surveyed repeatedly using high-precision GNSS measurements. The displacements of the borehole collars indicate a south-eastern flow direction with an azimuth of about  $155^\circ \pm 10^\circ$ . Besides determining the general flow direction from the absolute movements of the borehole collars, their relative displacements provided further insights. In Fig. 3, the displacements of the individual boreholes-borehole collars are plotted. The south-eastern boreholes (BH04 to BH07) show significantly smaller displacements, compared with the boreholes located in the north-western part of the array (BH01 and BH10 to BH12). This indicates compression of the ice in this region.

100

### 3 Ice flow modelling

To support these observations at the surface, the ~~conditions inside the glacier were investigated with a numerical~~ internal glacier dynamics was investigated by the means of a three-dimensional ice flow model. ~~We modelled the dynamics of the whole~~ A bedrock model and surface topographic information were used to determine the actual ice thickness of the glacier and to

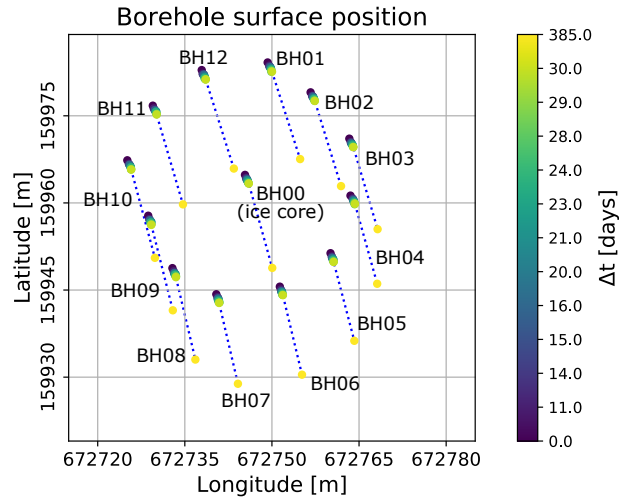
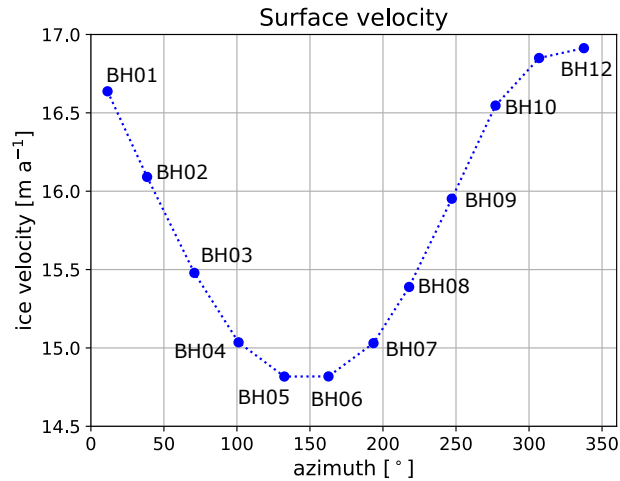


**Figure 2.** Analysis of ice flow direction, the displacement of the borehole surface points measured by GNSS is shown for each borehole with colours indicating the time since drilling.

Analysis of ice flow direction, the displacement of the borehole surface points measured by GNSS is shown for each borehole with colours



indicating the time since drilling.

**Figure 3.** The ice flow analysis shows the absolute horizontal displacement of the borehole collars from GNSS after 385 days for each borehole around the ice core hole (borehole azimuthal direction relative to ice core hole, N=0°).

105 constrain the model. The bedrock model was obtained from GPR measurements (Church et al., 2018) and from a Swiss-wide glacier inventory that is currently being updated (Farinotti et al., 2009; Grab et al., 2018). With the given information, we simulated the ice flow of Rhonegletscher using the Elmer/Ice model-modelling code (Gagliardini et al., 2013), which solves the full Stokes equations based on Glen's flow law .Here we simply ran the stationary model without any time evolution. Main

model inputs are a bedrock model and surface topographic information, as well as sliding coefficient (Glen, 1955) for the ice rheology, namely,

$$\dot{\epsilon}_{ij} = A(T) \tau^{n-1} \tau_{ij}, \quad (1)$$

where  $\dot{\epsilon}_{ij}$  is the strain rate,  $\tau_{ij}$  is the deviatoric stress, and  $\tau^{n-1}$  is the second invariant of the deviatoric stress tensor. The creep exponent  $n$  was chosen with  $n = 3$  as typical value for valley glaciers (Budd and Jacka, 1989). Basal sliding is modelled by using Weertman's friction law as boundary condition at the ice-bedrock interface:

$$u_b = c \tau_b^{\frac{1}{m}} \quad (2)$$

where  $u_b$  is the norm of the basal velocity,  $\tau_b$  is the basal shear stress, while  $m$  and rate factor  $c$  are constant parameters. The main model parameters are the coefficient  $c$  and the rate factor  $A$  that control the amount of basal motion and internal deformation, respectively. The bedrock model was obtained from GPR measurements (Church et al., 2018) and from a Swiss-wide glacier inventory that is currently being updated (GlaThiDa Consortium, 2019; Farinotti et al., 2009; Grab et al., 2018). As rate factor, we choose  $A = 100 \text{ MPa}^{-3} \text{ a}^{-1}$ , which was tuned for modelling Aletschgletscher (Jouvet et al., 2011) and a homogeneous sliding coefficient proved to correctly reproduce the velocities of Aletschgletscher (Jouvet et al., 2011). The rate factor is close to the literature value for temperate ice ( $76 \text{ MPa}^3 \text{ a}^{-1}$ ) (Cuffey and Paterson, 2010). As sliding coefficient, we used  $c = 10 \text{ km MPa}^{-1}$ . We tuned the sliding coefficient, which was tuned such that the observed and modelled ice velocities match at the surface of the borehole. As outputs from the Elmer/Ice model Additional bedrock velocity values with less than  $5 \text{ m a}^{-1}$ , estimated from borehole camera investigations (Gräff et al., 2017), supports our assumptions for this value. It is rather small compared to previous studies on Alpine glaciers (Jouvet and Funk, 2014; Compagno et al., 2019). Here, we ran the model in a stationary fashion without time evolution. As model outputs, we obtained the velocities-velocity and stress field in three dimensions. For a sensitivity analysis, we also tested different rate factors and basal sliding coefficients. As the model still slightly overestimated the derived basal velocities, we also analysed the case without basal sliding ( $c = 0 \text{ km MPa}^{-1}$ ). In this case, an extremely high rate factor  $A = 200 \text{ MPa}^{-3} \text{ a}^{-1}$  was required to fit the measured velocities. Furthermore, the principal stress axes did not change significantly. These changes lead to a slightly enhanced longitudinal simple shear component and slightly weaker longitudinal compressional component in the deepest parts of the ice. Therefore, we only considered  $A = 100 \text{ MPa}^{-3} \text{ a}^{-1}$  and  $c = 10 \text{ km MPa}^{-1}$  in the following analysis.

#### 4 Crystal Orientation Fabric Analysis

For detailed structural investigations of the temperate glacier ice, we performed a COF analysis was performed in the laboratories of the Alfred-Wegener-Institute Helmholtz Centre for Polar and Marine Research (AWI). We measured the orientation of the c-axes of the ice grains were analysed to determine the orientation of the crystals. The c-axis is the symmetry axis perpendicular to the basal plane of a hexagonal crystal. Along the c-axis, the physical properties, such as bulk and shear modulus, differ significantly from any direction parallel to the basal plane (the a-axes). The elastic parameters of the ice, such as bulk or

140 shear modulus, have enhanced values in the c-axis direction and the crystal is more resistant ~~against to~~ deformation (Cuffey and Paterson, 2010, chapter 3). This results in anisotropy effects, which ~~lead, for instance,~~ leads to different velocities for acoustic waves travelling through the ice (e.g. Diez and Eisen, 2015).

From the ice core extracted from the central borehole BH00 (Fig. 2), seven samples at depths of 2, 22, 33, 45, 52, 65 and 79 m were considered. Due to technical problems during the core retrieval, the azimuthal orientations of the samples at 2 and 45 m  
145 depth are subject to some uncertainties. Their azimuthal orientations were thus obtained from extrapolations from adjacent measurements.

Each of the seven samples consisted of an ice core segment of about 50 cm length. Up to four 11 cm long adjacent sub-samples (Fig. 4) were prepared from each of these segments. Each sub-sample was then further dissected into a horizontal and two vertical cuts, ~~all three~~. All three cuts are perpendicular to each other (Fig 4). This resulted in a horizontal circular slice and two  
150 vertical slices with SN- and EW-orientations from which thin sections were prepared. ~~Between~~ We measured between 8 and 12 thin sections per sample and 77 thin sections in total ~~were measured~~. This procedure enabled a more comprehensive analysis of the large crystals existing in temperate glacier ice (e.g. Kamb, 1959; Rigsby, 1960) and ~~fractures~~ a tracing of fissures (also called fracture traces), for instance from potential meltwater intrusions. The dimensions of the pieces were 10×6 cm for the vertical sections and a diameter of  $\approx 7$  cm for the circular horizontal sections. The creation of sub-samples and choosing three  
155 different types of sections (horizontal, EW-vertical, SN-vertical) for every sub-sample resulted in a comprehensive analysis of at least 300 grains for each depth level.

~~During the preparation of the ice thin sections, large-area scanning microscope (LASM) images (Binder et al., 2013; Krischke et al., 2015) were taken from the polished surface of the 1 thick ice samples. As discussed later, these images provide important information on the grain boundary network as well as the air bubble distribution, since light from the active camera is backscattered to a great extend by the evenly polished ice surfaces. Uneven parts, such as air bubbles or grain boundaries, reduce the amount of backscattered light and appear darker in the image.~~ All sections were analysed using ~~polarised~~ cross-polarised light (Wilson et al., 2003; Peternell et al., 2009). ~~The~~ We used the automatic fabric analyser G50 from Russell-Head Instruments (Wilson et al., 2003) ~~was used~~ to measure the orientation of the c-axis on a predefined mesh grid with a pixel resolution of 20x20  $\mu\text{m}^2$ . The orientation of the c-axis of an ice crystal is determined by two angles:  
160

$$165 \quad c(\vartheta, \varphi) = [\cos(\vartheta) \sin(\varphi), \sin(\vartheta) \sin(\varphi), \cos(\varphi)]. \quad (3)$$

The first angle defines the azimuth  $\vartheta \in [0, 2\pi]$  of the c-axis in the horizontal plane. The second angle is the colatitude  $\varphi \in [0, \frac{\pi}{2}]$  from vertical.

For the postprocessing of the obtained crystallographic data, we used the software *cAxes* (Eichler, 2013) ~~was used~~. *cAxes* analyses the misorientation angle between the determined c-axis orientations of neighbouring pixels and combines those with  
170 a misorientation  $< 1^\circ$  to individual ice grains with a mean c-axis azimuth and colatitude per grain. The minimum grain size, calculated from the number of pixels multiplied by the pixel resolution, was set to 0.2  $\text{mm}^2$  (500 pixels). ~~Vertical thin sections (Fig. 6, SN/EW) were rotated~~ cAxes automatically rotated vertical thin sections around the horizontal x-axis  $x'$  of the local measurement coordinate system  $(x', y', z')$  by  $90^\circ$  into the ice core system ( $z = \text{core's vertical axis}$ ) ( $z = y'$  and  $y = -z'$ ). Then,

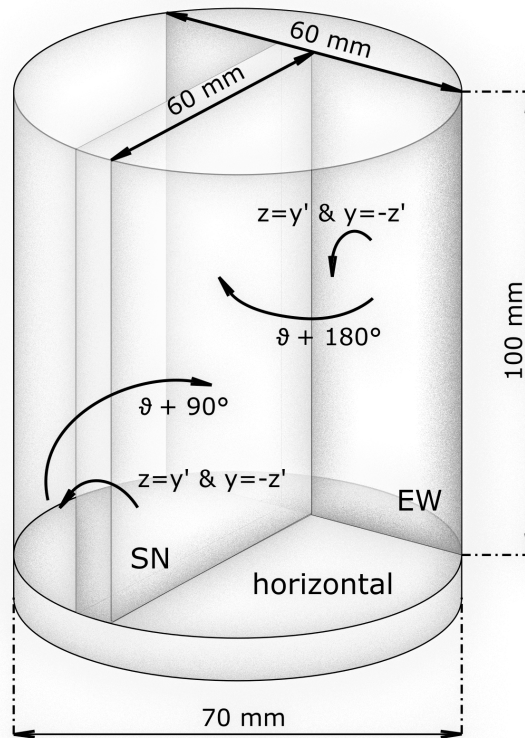


**Figure 4.** Cutting scheme for the ice core analysis. An 11 cm long piece of the ice core was cut in a horizontal (d=7 cm) and two vertical (east-west, south-north oriented, 10x6 cm) thin sections. Four thin sections of each type were analysed and combined per sampling depth.

175 they the thin sections were rotated towards the reference point that was engraved into the core segments (e.g.  $\theta_{EW} = \theta_{EW} +$   
 180°). In a final step, we used the magnetometer data ~~were used~~ to obtain the true azimuthal orientation for all thin sections  
 of a sampling depth relative to geographic north. This ensures an identical coordinate reference frame for all types of thin  
 sections along the whole ice core. Finally, we computed the eigenvalue distribution according to the procedure of Wallbrecher  
 (1986) ~~was computed~~. The three eigenvalues  $a_i \lambda_i$  ( $i=1, 2, 3$ ) follow the relations  $\sum a_i = 1$  and  $0 \leq a_3 \leq a_2 \leq a_1 \leq 1$   $\sum \lambda_i = 1$   
 180 and  $0 \leq \lambda_3 \leq \lambda_2 \leq \lambda_1 \leq 1$ . These eigenvalues represent the main axes of an ellipsoid which presents the best fit for a given  
 c-axis density distribution.

## 5 Results

Figure 5 shows the results of the COF analysis (left panels) and selected images of horizontal cross-polarised thin sections thin  
sections (right panels) for each depth level. The COF results are displayed in form of Schmidt equal-area stereo plots on the

lower hemisphere (vertical core axis in centre). Results from all sub-samples and section orientations are combined. Each ice grain c-axis is represented by a dot. As shown by the images ~~of cross-polarised thin sections~~ in the right panels of Fig. 5, the ice matrix is dominated by a few extremely large grains. Nevertheless, several hundred small grains appear along the grain boundaries or in specific patches. Especially the samples from 22 m and 45 m contain a large number of small grains. These grains form specific patterns looking like ~~fractures~~ fracture traces or fissures, which are traceable through several thin sections.

For better visualising the c-axis distributions, a smoothed colour density plot, calculated in accordance to Kamb's method (Vollmer, 1995), was superimposed on the stereo plots. These density plots only consider the number of grains within the area of the stereo plot, i.e. the size of the individual grains does not affect the colour code. All density plots indicate a multi-maxima pattern ~~-, whereby and~~ the majority exhibits four maxima. The orientation of the patterns varies with depth, but the structure inside the ~~pattern~~ patterns is remarkably similar. The four maxima lie on a small circle girdle, which is characterised by an opening angle around a central vector, shown as a ~~centroid~~ midpoint in the stereographic projection. Two maxima always lie on opposite sides of this ~~centroid~~ midpoint and the other two on a line perpendicular to the first two clusters so that the azimuthal ~~distribution~~ separation of the maxima is  $90^\circ$ . Deviations are observed at 45 m depth, where a fifth maximum at the horizontal margin appears, and at 79 m, where one of the four maxima is significantly weaker than the others. Depending on the number of grains per cluster the midpoint (red point in Fig. 7) differs from the actual centroid (blue dot) of the multi-maxima pattern.

The opening angle between the midpoint and the individual maxima varies with  $\pm 15^\circ$  around a mean of  $30^\circ$  (Table 1), but the mean value is constant over all depths.

The eigenvectors of the polycrystalline orientation tensor were calculated for each depth, and they are also shown in the stereo plots (blue dots in Fig. 5). For ~~an~~ enhanced visibility, the ~~normal plane for~~ plane normal to the eigenvector associated with the largest eigenvalue  $\lambda_1$  is indicated with a dashed blue line. This eigenvector ~~is plotting in the centre of the four-point maximum.~~

~~The opening angle between the largest eigenvector and the individual maxima varies with  $\pm 15$  around a mean of  $30$  (Table 1), but the mean value is constant over all depths~~ coincides with the centroid of the four-point-maxima. The other two eigenvalues are significantly lower than  $\lambda_1$  ( $0.56 \leq \lambda_1 \leq 0.7$ ) and usually in a range of  $0.1 \leq \lambda_2 \leq 0.31$  and  $0.09 \leq \lambda_3 \leq 0.13$ , respectively.

With an exception for the uppermost depth at 2 m ~~and the lowermost depth at 79 m,~~ the ~~COF patterns in the upper part of the ice core are oriented in~~ azimuth of the maximum eigenvectors ( $147^\circ \pm 31^\circ$  is aligned with the direction of the glacier's ice flow ~~(e.f.  $155^\circ \pm 10^\circ$ , cf. Figs. 1, 2).~~

With increasing depth, the ~~centre of the e-axis distribution~~ maximum eigenvector has a decreasing colatitude, and at 79 m ~~the largest eigenvector~~ this eigenvector as well as the centroid of the cluster is almost vertically oriented.

For an enhanced and statistically significant data set, we combined the determined c-axis orientations, measured in up to twelve individual thin sections with three different orientations. However, the results from the different orientations of the sections (Fig. 4) may be inconsistent. Although the grains are not elongated in a certain direction (i.e. do not show a shape preferred orientation), some of them appear branched and interlocked (Fig. 5, right panels). Therefore, two-dimensional cuts through large, branched grains may let them appear as several individual grains within the same section. ~~This~~ Kamb (1959) and Hooke (1969) have already discussed the statistical relevance of these branched grains. The sketch in Hooke and Hudleston (1980)

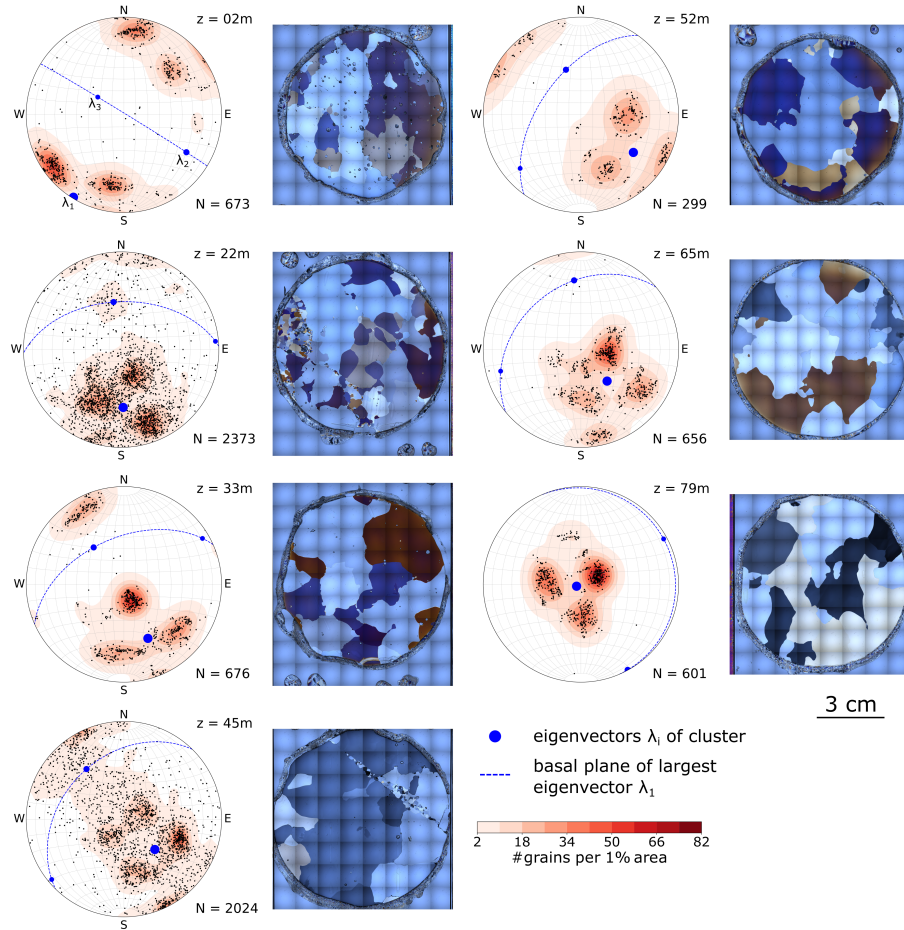


**Figure 5.** Left columns: Stereo plots (lower hemisphere Schmidt equal-area projection into the horizontal, i.e. long axis of core is-plots in the centre) with the final-c-axis distribution and associated horizontal thin sections, illustrating the typical grain size distribution, are shown for each sample. The total number of ice grains ( $N$ ) is specified for each sample (consisting of at least 3 horizontal and 6 vertical thin sections, all rotated to horizontal view and common geographic coordinates). The sampling depth ( $z$ ) is indicated in-at the upper right corner of the stereo plots. The colour code (smoothed Kamb's distribution (Vollmer, 1995)) emphasises the existing clusters of the c-axis distribution. The largest eigenvector for the determined distribution is depicted as blue dot and its normal plane is shown as dashed line. Right columns: example images of horizontal thin sections, recorded under cross-polarised light

**Table 1.** Angles between individual maxima and the centroid, i.e. the largest eigenvector, describing the relative geometry of the multi-maximum-multi-maxima pattern and the absolute position-orientation (azimuth/colatitude) of the centroid.

depth [m]	relative angles within the cluster					absolute position of cluster	
	angles per maximum [°]				mean angle [°]	azimuth [°]	colatitude [°]
2	23.3	27.4	34.3	34.5	$29.9 \pm 4.7$	211.5 (151.5)	88.6
22	23.5	25.3	34.5	35.2	$29.6 \pm 5.2$	178	49.4
33	20.8	26.0	41.0	47.6	$33.9 \pm 10.9$	156	50.6
45	26.9	29.2	30.7	33.2	$30.0 \pm 2.3$	134.4	36.6
52	22.2	27.9	29.6	38.2	$30.6 \pm 5.7$	125.6	55.7
65	20.6	22.5	34.7	37.6	$28.9 \pm 7.4$	140.2	34.5
79	20.2	25.2	34.3	34.6	$28.6 \pm 6.1$	246.6	3.9

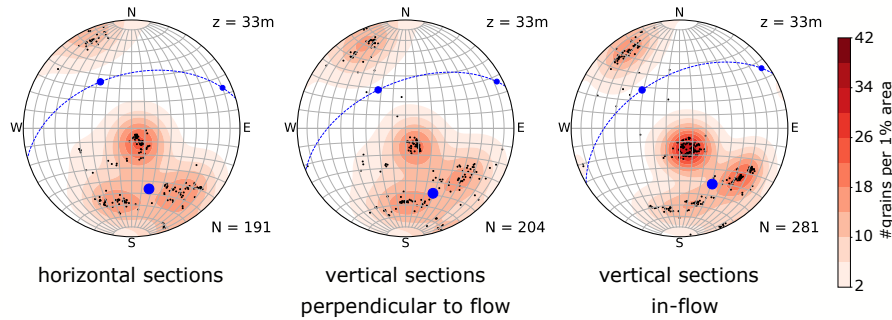


**Figure 6.** Stereo plots (lower hemisphere Schmidt equal-area projection) for the three types of sub-samples (horizontal, east-west, south-north, from left to right) - Number of grains  $N$  is given for each type of sub-sample. The colour code (smoothed Kamb's distribution (Vollmer, 1995)) emphasises the maxima of the c-axis distribution. The blue dot indicate the largest eigenvector and the dashed blue line indicate its normal plane with annotations as in Fig 5.

220 , Fig. 6, and more recently in Monz et al. (2020), Fig. 3, further illustrate this issue that could result in over-represented clusters in individual thin sections, which appear in the superimposed stereo plots from the different sub-samples.

To check the consistency of the individual orientations, the c-axis distribution for each sub-section (horizontal, east-west and south-north) was analysed separately. Figure 6 shows the results for the sample at 33 m depth. All three sub-sections show a similar pattern. The individual maxima appear in all sections and are not a result of stitching differently orientated sections together. However, due to the afore-mentioned reasons, the actual grain size is difficult to determine. Individual analyses for  
225 the other depths showed similarly consistent results (not shown).

## 6 Interpretation

The results, shown in Fig. For our interpretation, we refer to the deviatoric stress tensor elements shown in Table 5, exhibit fairly consistent patterns that can be explained in terms of glacier dynamics. Here2. The x-component of the tensor elements is aligned with the longitudinal direction, i.e. the glacier flow, and the y-component is aligned with the transverse direction. Due to the flow evolution of the ice grains through the glacier, these grains are deformed under given stress conditions (Schulson and Duval, 2009, chapt. 5). As the glacier changes its flow direction, the ice crystals experience changing stress conditions leading to variations in the deformation regime. As a result, the c-axes of the ice grains are oriented in specific patterns, such as the multi-maxima structure that we observed in the current ice core. Stress and strain are directly linked via Glen's flow law and changing stress causes a change in deformation geometry. However, the particular orientation of ice grains is crucial as to whether the ice is easy to deform ("soft" direction) or whether it is further resistive ("hard" direction) against the currently applied deformation. For a detailed analysis of the current stress conditions at the ice core location, we use the ice flow model to derive the Cauchy stress, i.e. the deviatoric stress tensor. The deviatoric stress tensor  $\sigma^{(d)}$  is derived from

**Table 2.** Stress tensor elements obtained from ice flow modelling (x – longitudinal, y – transverse, z – vertical direction).

depth [m]	$\sigma_{xx}^{(d)}$ [MPa]	$\sigma_{yy}^{(d)}$ [MPa]	$\sigma_{zz}^{(d)}$ [MPa]	$\sigma_{xy}^{(d)}$ [MPa]	$\sigma_{xz}^{(d)}$ [MPa]	$\sigma_{yz}^{(d)}$ [MPa]
2	-0.087	0.037	0.050	-0.026	0.024	0.004
22	-0.079	0.037	0.042	-0.026	0.040	0.003
33	-0.074	0.036	0.038	-0.025	0.048	0.003
45	-0.068	0.034	0.033	-0.024	0.057	0.004
52	-0.063	0.033	0.030	-0.024	0.062	0.004
65	-0.054	0.030	0.025	-0.022	0.071	0.004
79	-0.043	0.026	0.018	-0.021	0.080	0.005

the normal stress tensor  $\sigma$  by subtracting the hydrostatic pressure  $p$  from its main diagonal elements, i.e.

$$\sigma_{ij}^{(d)} = \sigma_{ij} - p\delta_{ij} \quad (4)$$

where  $\delta_{ij} = 1$  for  $i = j$ , and  $\delta_{ij} = 0$  otherwise. For the deformation of the ice grains only the deviatoric stress tensor is important. The two most relevant components at the core location are the longitudinal compressional stress  $\sigma_{xx}^{(d)}$  and the longitudinal shear stress  $\sigma_{xz}^{(d)}$  (Table 2).  $\sigma_{xx}^{(d)}$  is the most dominant stress close to the surface. Its strength slightly decreases with depth. In addition, the simple shear  $\sigma_{xz}^{(d)}$  governs the stress conditions in deeper parts as it increases with depth. The transverse components ( $\sigma_{yy}^{(d)}$ ,  $\sigma_{xy}^{(d)}$  and  $\sigma_{yz}^{(d)}$ ) are more or less equal in all depths. In addition to the stress components, we also calculate the strain rates  $\dot{\epsilon}_{ij}$  from the stress tensor by using Glen's flow law, i.e. (1). To constrain these calculations we also compute the strain rates for the two dominant components  $\dot{\epsilon}_{xx}$  and  $\dot{\epsilon}_{xz}$  from our borehole data set. All values are shown in Table 3. These data were derived from borehole inclination measurements within 4 weeks in summer and upscaled for annual strain rates. Smaller changes

**Table 3.** Strain rates derived from borehole measurements and from ice flow modelling (x – longitudinal, y – transverse, z – vertical direction).

depth [m]	modelled strain rates						borehole experiments	
	$\dot{\epsilon}_{xx}$ [a <sup>-1</sup> ]	$\dot{\epsilon}_{yy}$ [a <sup>-1</sup> ]	$\dot{\epsilon}_{zz}$ [a <sup>-1</sup> ]	$\dot{\epsilon}_{xy}$ [a <sup>-1</sup> ]	$\dot{\epsilon}_{xz}$ [a <sup>-1</sup> ]	$\dot{\epsilon}_{yz}$ [a <sup>-1</sup> ]	$\dot{\epsilon}_{xx}$ [a <sup>-1</sup> ]	$\dot{\epsilon}_{xz}$ [a <sup>-1</sup> ]
2	-0.061	0.026	0.035	-0.018	0.017	0.002	-0.043	-0.002
22	-0.056	0.026	0.030	-0.018	0.028	0.002	-0.062	-0.009
33	-0.053	0.026	0.027	-0.018	0.034	0.002	-0.062	-0.004
45	-0.049	0.025	0.024	-0.018	0.041	0.003	-0.059	-0.005
52	-0.047	0.024	0.023	-0.017	0.046	0.003	-0.054	+0.006
65	-0.042	0.023	0.019	-0.017	0.055	0.003	-0.032	-0.002
79	-0.036	0.021	0.014	-0.017	0.065	0.004	+0.015	+0.084

might be levelled out as they are smaller than the measurement accuracy and the sensitivity of the instruments. Additionally, the glacier flow may fluctuate over the seasons. Therefore, we consider these data just as supporting values.

250 In the following, we provide an interpretation of three significant features presented in Fig. 5, namely

- the azimuthal orientation of the c-axes distributions as represented by the maximum eigenvectors,
- the decrease of the e-axis-maximum eigenvector colatitudes with increasing depths (viz. this eigenvector becomes more vertical), and
- the existence of multi-maxima patterns in the c-axis distributions.

255 To aid support the interpretation, the stereo plots in Fig. 5 are shown again in Fig. 7 with adjustments as a result of the following interpretation. Here, only the colour-coded c-axis density distributions are plotted, superimposed by additional information obtained from accompanying analyses.

## 6.1 Azimuthal orientation

Results from all depth levels, with the exception for 2 m (Fig. 5), show in general a mean c-axis orientation (Table 1) approximately parallel to the main glacier flow direction that was obtained from the displacements of the surrounding boreholes (Fig. 2,  $\approx 155^\circ$ ). As a result of the horizontal compression ( $\sigma_{xx}$ ), determined from the relative movements of the surrounding boreholes The largest eigenvector  $\lambda_1$  always lies in a vertical plane that is aligned ( $\pm 20^\circ$ ) with the glacier flow direction. This flow kinematics, depicted by the principal stress axis (Fig. 3), the azimuths and 7) causes an alignment of the centroid of the c-axes are aligned with the azimuth of this compressional stress. This with the current ice flow. As this flow direction changes, the COF have most likely developed in the last four decades since the glacier flows in the direction observed at our drill location. Although the centroid in 79 m is vertically oriented, the characteristic “diamond shape“ of the multi-maxima pattern is still joining the vertical plane of the glacier flow direction (the verticality of the pattern is discussed below).

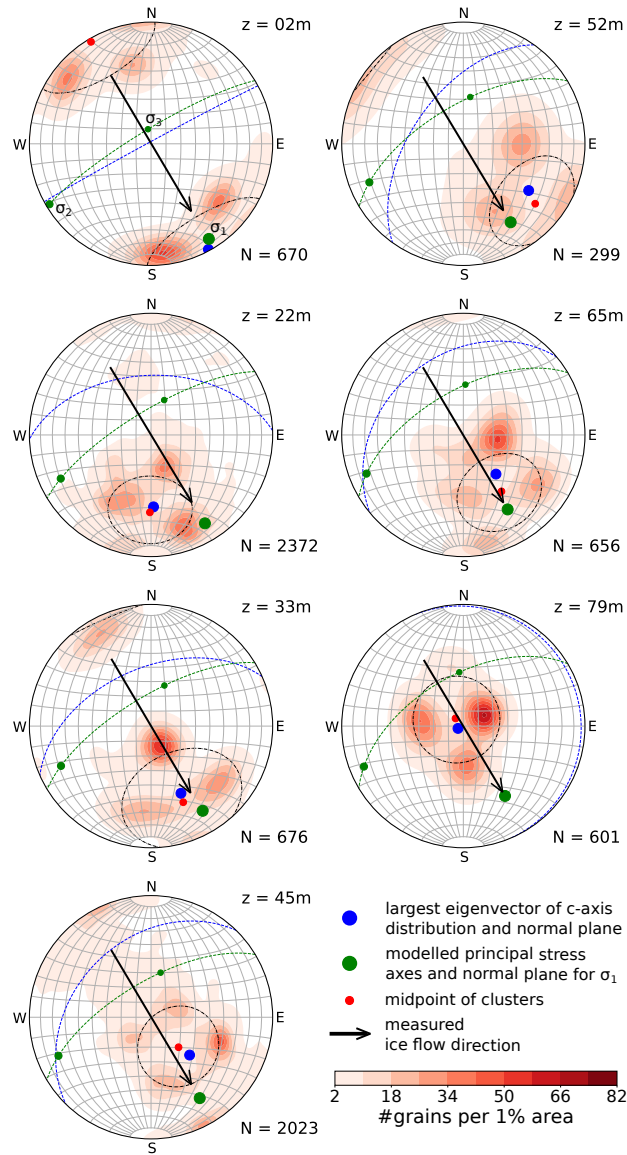


**Figure 7.** Stereo plots (lower hemisphere Schmidt equal-area projection) with the colour coded (same as Fig. 5) c-axis distribution for each sample are shown. Note: The azimuth for  $z=2$  m is corrected by  $-60^\circ$  (see text for discussion). The total number of ice grains is specified for each sample. The black dashed line shows the mean opening angle for the cone of maxima around the centroid depicted as red dot. The calculated largest eigenvector for the c-axis distribution is shown as blue dot (its normal plane as dashed blue line) and the calculated largest compressional principal stress axis from the ice flow model is represented by a green dot (its normal plane as dashed green line).

This observation is in accordance with results from laboratory experiments in a number of previous studies (e.g Kamb, 1972; Duval, 1981; Budd and Jacka, 1989) and comparable with some parts of the Cape Folger ice core (Thwaites et al., 1984).  
270 The uppermost sample (2 m) does not fit into this interpretation. Although the magnetometer data are consistent, the onset core break between two segments at 10 m was unclear and we cannot fully exclude a misorientation between the segments in 2 and 22 m. As shown in Fig. 7 an azimuthal correction of  $-60^\circ$  would lead to a perfect alignment of this sample with all other observation-observations and the modelling results for the particular location. Therefore, we assume a misorientation of the core segments. ~~However, the orientation of the pattern in 2 is in alignment with the glacier flow about 800-1000 up glacier~~  
275 ~~(Fig. 1). As the absolute stress and strain rates are lower at the surface, the pattern close to the surface might not be reshaped in the last 1000 of ice flow and thus show the remnant orientation further up glacier when the ice was buried deeper in the glacier and thus exposed to higher absolute stress and strain rates.~~

## 6.2 Colatitude variations

HereIn the following, we consider the variations of the colatitude of the largest eigenvector  $\lambda_1$  (Fig. 7, blue dot). There is a decrease of the colatitude from  $89^\circ$  to  $4^\circ$  with increasing depth (Table 1). ~~This is likely~~ Considering the deformation mechanisms, mainly dislocation creep, this is the result of the stress and strain distribution-rate distribution (Tables 2 and 3) in the glacier. Generally, the ice crystal c-axes of the ice crystals orient themselves parallel to the ice flow, which coincides with the modelled maximum compressive stress-compressional principal stress direction ( $\sigma_1$ ) direction in Fig. 7). As indicated by the relative movements of the surrounding boreholes (Fig. 3), we indeed observe a compression parallel to the glacier flow at the glacier  
285 surface. ~~Based on~~ In accordance with borehole inclination measurements ~~(not shown), it can be further assumed that and the derived strain rates (Table 3),~~ the flow-parallel compression also occurs at greater depths ~~. However but slightly decreases. In contrast,~~ with increasing depths, the ice overburden generates an additional vertical stress component. This causes an increasing vertical depth, the shear stress significantly increases. Especially in the deepest parts of the ice core, the longitudinal simple shear component  $\sigma_{xz}^{(d)}$  governs the stress state, which is also confirmed by the inclinometer measurements. This increasing  
290 shear deformation of the ice ~~which lets the c-axes rotate towards a vertical direction lets the colatitude angle decrease~~ with increasing depths, and explains, at least qualitatively, the observations in Fig. 7.

The ~~principle compressive stress orientations~~ principal stresses ( $\sigma_1$ ), modeled with the Elmer/Ice  $\sigma_2, \sigma_3$ ), derived from the ice flow model, were added to Fig. 7 (green dots ~~in the stereo plots~~) for comparison. Although not matching perfectly, we observe a generally good agreement between modelled and observed largest eigenvector directions (blue dots) is observed  
295 in Fig. 7, thereby the largest eigenvector  $\lambda_1$  and the dominant principal stress  $\sigma_1$  supporting our interpretation. ~~However, the discrepancy might be a hint~~ The discrepancy especially for the deepest sample is considered as evidence that the c-axis distribution is governed by strain (and not stress) in the last consequence (Budd et al., 2013; Faria et al., 2014b). Especially in (Budd et al., 2013; Faria et al., 2014b; Weikusat et al., 2017). In the presence of simple shear, the direction of stress and strain are not necessarily aligned anymore, in particular for recently formed ice grains the principal stress axis and principal strain  
300 axis are not aligned (non-coaxial relation) (Duval, 1981). This implies that the COF for the deepest sample is dominated by simple shear. According to our strain rate components (Table 3) such an implication is justified. The modelled shear strain rate

is twice as large as any other component and causes the most significant effect in the borehole measurements after a short time period.

### 6.3 Multi-maxima c-axes distribution

305 If the c-axis orientations would be governed solely by the orientation of the ~~principal compressive stress~~ major principal stress and strain direction ( $\sigma_1$ ), ~~we should observe (mainly a result of compressional and simple shear stress),~~ we would rather expect a single maximum in the stereo plots as in the deepest part of other ice cores (Faria et al., 2014a). However, as observed in Figures 5 and 7, this is clearly not the case. Instead, the orientations deviate on average about  $30^\circ$  from the ~~principle~~ principal stress direction (indicated by black ~~circles~~ small circle girdles in Fig. 7).

310 ~~A possible explanation of this observation includes~~ The most likely reason for this observation involves recrystallisation processes. ~~As described in Duval and Castelnau (1995) and Schulson and Duval (2009, chapter 6), it can be distinguished between rotation recrystallisation, which is observed primarily in cold ice (e.g. Lipenkov et al., 1989), and migration recrystallisation, which seems to be the dominant mechanism in temperate ice near the pressure melting point (e.g. Gow and Williamson, 1976; Azuma and F~~

315 ~~. In a more recent work~~ For our interpretation we follow the approach of Faria et al. (2014b), these processes are no longer just attributed to temperature, but to temperature in combination with cumulative strain and the term dynamic recrystallisation is used. In any case, dynamic grain growth and the formation of new nuclei are dependent on temperature, as the grain boundary mobility depends on the general energy state of the system, and strain rate due to dislocations being formed during deformation. Under constant strain rates, higher temperatures cause an increased grain growth (Schulson and Duval, 2009, chapter 6) and a faster recrystallisation in case of inadequately oriented grains and heterogeneous distribution of dislocations in neighbouring

320 grains (Weikusat et al., 2009b, Fig. 8). ~~As explained in Cuffey and Paterson (2010, chapter 3), c-axis orientations, resulting from migration recrystallisation tend to deviate from the principle compressive stress direction ( $\sigma_1$ ), as observed in Fig. 7. If the recrystallisation would be the result of an unconfined compression only, one should observe a continuous distribution of the c-axes along the small circle girdle (black circles in Fig. 7). Instead, the orientations typically cluster around four maxima lying on these circles. As shown in Figure 3.7 in Cuffey and Paterson (2010, chapter 3), this can be explained by~~

325 ~~a combination of compressional and shear stresses. The modelled stress tensor provides hints for increasing shear stresses ( $\tau_{xz}$ ) with depth, and also borehole inclination measurements provide some evidence for the occurrence of shear stresses. The borehole trajectories of all 12 boreholes around the core location show typical parabola-shaped curvature 50 below the surface four weeks after drilling. Our interpretation is based on the assumptions that (i) who distinguish between three types of recrystallisation: rotational recrystallisation (RRX), and two very similar but significantly different types of strain-induced~~

330 ~~boundary migration (SIBM) occurs in the investigation area, and (ii) that all crystals have been recrystallised recently. The former requires temperatures near the pressure melting point. Concerning the later and following the most recent research of Faria et al. (2014b), a change in the strain rate due to different flow direction in the glacier would lead to a grain size reduction regime. The existing grains start to recrystallise, and the newly~~ The first type assumes that under given strain conditions, already existing (i.e. old), suitably oriented grains grow until they reach again the steady-state, which depends on temperature,

335 ~~grains size and strain rate (which is directly related to stresses in magnitude). As this is a continuously ongoing process, we~~

can expect a direct relationship between current stress and thus strain rate and the orientation under constant temperature conditions. This interpretation is also in good agreement with findings in Budd and Jacka (1989). Evidence that the crystals must have formed near the pressure melting point, can be found in the images of cross-polarised thin section (right panels in Fig. 5) and in the grain size distribution provided in Table 4. Evidently, our samples include very large crystals, and there is a considerable variability of the grain sizes at all depths. This is indicative for crystal formation near the pressure melting point (Gow and Williamson, 1976; Jacka and Jun, 1994), which in turn allow an extremely fast grain growth (Alley, 1992). These observations are further supported by derived temperature profiles in a 25 deep tunnel close to the glacier snout clearly indicating temperate conditions of  $> -1$  (personal comm. M. Lüthi, 2019). Supporting arguments for a fast and complete dynamic recrystallisation of the individual grains are provided by the distribution of air bubbles, found in the LASM images. An example of a LASM scan, obtained from 2 depth, is shown in Fig. ?? . It exhibits bubble-free (top part) and bubble-rich (bottom part) areas. Similar distributions were found at other depth levels, although the amount of air bubbles generally decreases with increasing depths. In polar ice, air bubbles are usually found along grain boundaries. They often migrate, when ice grains are growing (Alley et al., 1986), as they can be regarded as an energetic obstacle in the crystal lattice. In the LASM scans in Fig. ?? , such air bubbles are observed as well (encircled with dashed red lines). However, there are also bubbles completely trapped within the ice grain matrix (encircled with dashed green line) and some air bubbles, which are still part of the grain boundaries, but causing a bending of these boundaries and the development of new sub-grain boundaries on the opposite side of the air bubble (encircled with dashed blue line). The later two air bubble types are evidence for an extremely fast boundary migration process and fast growing ice crystals. Stereo plots (lower hemisphere Schmidt equal-area projection) with the colour coded (same as Fig. 5) final c-axis distribution for each sample are shown. The total number of ice grains is specified for each sample. The black dashed line shows the mean opening angle for the cone of maxima around the centroid depicted as red dot. The calculated largest eigenvector for the c-axis distribution is shown as blue dot (its normal plane as dashed blue line) and the calculated largest principal stress axis from the ice flow model is represented by a green dot (its normal plane as dashed green line). at the cost of less suitably oriented grains (called SIBM-O). The second type is very similar, but with a relevant difference: when the grain grows parts at the boundaries like bulges can be nuclei for new smaller grains (therefore called SIBM-N, see an exemplary process described by Steinbach et al. (2017) with a very similar orientation like their parent grain. These new grains are considered as strain-free grains and have an impact on the grain size.

In our data set we observe a variety of different grain sizes. Table 4 summarises the grain size distribution in our ice core samples. As mentioned earlier, the two-dimensional cuts through the ice core samples may lead to a misinterpretation of the grain sizes as large interlocked grains can appear as several small grains. However, it can be expected that not all small grains are cut branches of large grains. We also analysed the COF for six different grain size classes individually. The data are shown in Fig. 8 for one sample (other samples in the supplement). The multi-maxima pattern is persistent in all grain size classes. Based on these findings, we postulate that this pattern is a result of SIBM-N in combination with the described longitudinal compressional and shear stress.

However, our data set cannot conclusively explain the very regular distribution of c-axes, i.e. the "diamond-shape", within the multi-maxima pattern.

**Table 4.** Grain size distribution (median, mean, and maximum grain sizes [ $\text{mm}^2$ ], minimum grain size is  $0.2 \text{ mm}^2$  and defined as threshold during processing) and number of grains within defined grain size classes [ $\text{mm}^2$ ].

depth [mm]	number of grains	median	mean	max	number of grains per class					
					<1	1-5	5-20	20-100	100-500	>500
2	673	5.30	77.06	1826.71	211	123	102	135	76	26
22	2373	0.79	19.04	1551.97	1340	584	192	165	69	23
33	676	4.41	85.97	3994.17	202	146	110	106	83	29
45	2024	0.88	29.89	3249.29	1078	522	173	133	91	27
52	299	14.67	121.42	1986.70	52	56	49	66	55	21
65	656	6.01	95.02	3752.65	195	119	123	112	67	40
79	601	6.81	96.79	3236.18	141	134	109	111	79	27

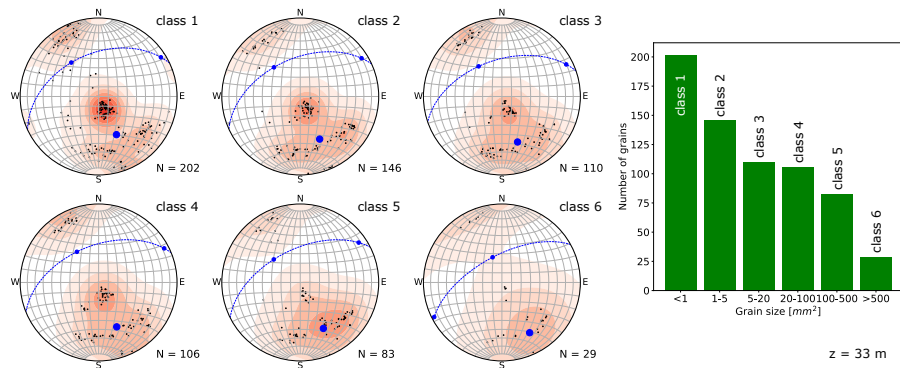


**Figure 8.** Example of a LASM image indicating several processes in the temperate ice: black areas are air bubbles and black lines represent Stereo plots (lower hemisphere Schmidt equal-area projection) with the grain boundaries colour coded (same as Fig. 5). Black dashed lines indicate subgrain boundaries. Air bubble-rich ice and air bubble-free ice have relatively sharp boundaries. Each plot represents a grain size class as indicated by the dashed orange line upper right corner. The number of grain boundaries (red circles in zoomed image) but also completely trapped within individual large ice grains (green circle in zoomed image) per class is specified for each plot. An intermediate state of incorporating air bubbles. The calculated largest eigenvector for the c-axis distribution is shown in the as blue circle dot (its normal plane as dashed blue line). Right column: histogram showing the number of grains per class.

## 7 Discussion

The literature on COF field studies is not conclusive concerning the existence of multi-maximum-multi-maxima fabrics. They were observed in early studies on temperate glaciers (e.g., Rigsby, 1951; Kamb, 1959; Rigsby, 1960; Hooke and Hudleston, 1980) (e.g., Rigsby, 1951; Kamb, 1959; Rigsby, 1960) for the first time. In the 1970's to 1980's, they have been found in ice capes with ice temperatures above  $-10^\circ \text{C}$  (Hooke and Hudleston, 1980), and also in the bottom ice of Byrd Station and Cape Folger in

375

Antarctica (Gow and Williamson, 1976; Thwaites et al., 1984) ~~and often referred as "diamond-shape" pattern or fabrics~~. At that time, the estimation of c-axis distributions was more subjective and could not benefit from modern equipment, ~~as employed in our study~~. The orientation of crystals was determined manually on a Rigsby-stage by turning and tilting the ice samples between polarised plates. Thus, only a limited number of grains (up to 100) and usually the largest grains were analysed.

380 Therefore, the ~~"diamond-shape"~~ pattern was debated to be a statistical or method-immanent effect. Interestingly, in more recent studies on other temperate glaciers ~~multi-maximum multi-maxima~~ fabrics in combination with a large grain size were only observed in the deepest parts of the ice cores (e.g. Tison and Hubbard, 2000). ~~However, following the argumentation in Faria et al. (2014b), strain-induced boundary migration (SIBM) and grain growth is not a result of temperature alone. Grain growth and the formation of new grains depends on temperature and strain rate. Most likely, the observed "diamond~~

385 ~~shape" pattern only develops under strain-induced boundary migration from new grains (SIBM-N) at high strain rates, in contrast to SIBM-O which already takes place at lower strain rates (under similar high temperature conditions) and in which the old grains are still in place (Faria et al., 2014b, Fig.13+14) drilled in the ablation zone (e.g. Tison and Hubbard, 2000). The conditions for a "diamond-shape" pattern seem to be suitable in larger large glaciers like the Rhonegletscher, whereas in smaller and thinner glaciers, such as Glacier de Tsanfleuron investigated in Tison and Hubbard (2000), the strain rates~~

390 ~~might be smaller due to the lower ice thickness and thus the multi-maxima patterns develop only in the deepest parts with presumably the highest with high~~ strain rates. In contrast, in polar ice cores the strain rates are expected to be large enough ; ~~but too, but a multi-maxima fabrics has been observed~~ only in the deepest parts ~~also the temperature conditions are fulfilled for multi-maximum fabrics as observed in of~~ some Antarctic and Greenlandic cores (Gow and Williamson, 1976; Thwaites et al., 1984; Montagnat et al., 2014). ~~There, the temperature conditions are similarly high as in temperate glaciers like the~~

395 ~~Rhonegletscher. The results of Thwaites et al. (1984) for the multi-maximum multi-maxima ice at the base of Cape Folger ice core show the largest similarities (orientation in relation to observed stresses, grain size structure, and the opening angle of the multi-maximum multi-maxima structure) with our results. To sum up this argumentation, multi-maxima patterns only form under high temperatures and high strain rates (SIBM-N case). Only if a certain strain rate is applied to the ice, the pattern is created in alignment with the deformation. This may explain why the COF at the depth of 2 (Figure 5) does not align with the~~

400 ~~current glacier flow. The absolute strain rate close to the surface is expected to be lower than deeper in the ice. Presumably, this strain rate at the current location is too low for a SIBM-N to take place and thus the previous orientation when the ice was buried deeper in the glacier and exposed to higher strain rates is preserved. The orientation fits to the flow about 800 up glacier. In contrast, COF laboratory experiments provide clear evidence for multi-maximum fabrics. Kamb (1972); Duval (1981) multi-maxima fabrics. Kamb (1972) and Maohuan et al. (1985) performed laboratory experiments on artificial ice under high~~

405 ~~temperatures (> -2°C), slightly below the pressure melting point. They combined shear and compressional stresses in their torsion-compression-experiments. This is similar to what we expect on Rhonegletscher. In another study, Duval (1981) argued that the multi-maximum centroid is parallel with the compressional axis, but he added that two further maxima exist that are parallel to the poles of the two main shear stress plains (vertical and horizontal). Maohuan et al. (1985) applied only a compressional stress onto the sample and showed a development of the structures from a small girdle around the compressional~~

410 ~~axis at early stages that developed towards a multi-maximum fabric~~ These experiments provide evidence that the main principal

stress determines the azimuth of the COF pattern. In addition ~~to that~~, the opening angles ~~we observe~~, we observe, fit quite well to the results of Jacka and Maccagnan (1984) who analysed the opening angle of small circle girdles formed under compressional stress. For such opening angles between compressional direction and the c-axis direction, the compressive strength applied onto the ice crystal is minimised (Schulson and Duval, 2009, chapter 11).

415 ~~The stresses applied on the samples in~~ As a result of these laboratory experiments ~~are in a similar range ( $\sigma = 0.24-0.6$  (Duval, 1981)) as what we expect from our glacier model for the intermediate and deeper parts (up to 0.7).~~ As the crystal orientation in these experiments adopted rather quickly towards new stresses under similar temperature and stress and field measurements, we conclude that the conditions in Rhonegletscher with high strain rates and high temperatures are an prerequisite for the development of multi-maxima patterns. Thus, a multi-maxima pattern is not necessarily found in all temperate glaciers.

420 Recrystallisation has regularly been observed in a variety of ice cores (Alley, 1988; Duval and Castelnau, 1995; Weikusat et al., 2009b; Sch  
. In most of these papers, two types of recrystallisation have been considered, namely rotation recrystallisation (RRX) and migration recrystallisation (Alley et al., 1995). As explained in detail in Faria et al. (2014b), this distinction bases on the so-called tripartite paradigm. They argue that this assumption is insufficient with respect to the mechanisms driving forces and introduce a new scheme to distinguish between different types of dynamic recrystallisation: RRX, which has been described

425 in detail in Alley (1988) and two types of strain-induced boundary migration (SIBM). RRX accounts for up to 10% of the recrystallisation processes observed in ice. Usually the shape of the ice grains is rather convex and RRX counteracts against the dynamic grain growth (Weikusat et al., 2011b). For SIBM, Faria et al. (2014b) distinguished between the two types SIBM-O and SIBM-N. In both cases, grains with less dislocations grow at the cost of grains with a large amount of dislocations. For SIBM-O an already existing grain grows further and further. In case of SIBM-N new small and strain-free grains nucleate from

430 the original parent grain (often along the grain boundaries) and start to grow on their own. Both mechanisms are driven by reducing the thermodynamic energy of the whole system and grains with heterogeneously distributed dislocations are absorbed (Weikusat et al., 2009b, Fig. 8) However, when considering the effect on the COF, these two mechanisms may lead to different COF. For SIBM-O a few very large grains would develop and under given strain and temperature conditions, we ~~can expect to have a similar fast adaption in the glacier. Thus, our findings are in good agreement with these laboratory experiments. Stereo~~

435 plots (lower hemisphere Schmidt equal-area projection) with principal axes of the c-axis eigenvectors (shown as blue dots), the normal plane for the largest eigenvector (repr. by the blue dashed line) and the plane of simple shear stress and the auxillary plane (perpendicular to the plane of simple shear) with their respective normal vectors (shown as dashed lines and dots in grey colours). Following Cuffey and Paterson (2010), we argue that the existence of would expect a single maximum pattern created by the most favourably oriented grains. For SIBM-N we regularly generate new grains with a similar orientation like

440 the parent grain. Furthermore, these new grains are strain-free and also start to grow. Therefore, we have certain concurrent maxima. This interpretation is further supported by the very heterogeneous grain size distribution with large, extremely branched grains and surrounding smaller grains with a similar orientation. These branched grains might be the parent grains surrounded by their nuclei. Temperature and strain rate conditions determine which recrystallisation mechanism dominates and the recrystallisation mechanism determines the grain size and shape. For high temperatures and strain rates, SIBM-N

445 is the dominating process according to Faria et al. (2014b, Fig. 13+14). This nucleation of new grains, which inherit the

orientation of their parent grains, could lead to the observed multi-maxima fabrics is the result of combined compressional ( $\sigma_{xx}$ ) and shear stresses ( $\tau_{xz}$ ). This hypothesis is also supported by microdynamical models (Llorens et al., 2016) and laboratory investigations (Journaux et al., 2019). These investigations provide evidence that simple shear processes in temperate ice produce two maxima, one perpendicular to the shear plane (parallel to the normal vector of that plane) and a second maximum in the direction of shearing. The exact angle between these two maxima depends on the experimental conditions (Qi et al., 2019). Such a horizontal shear plane and its normal vector ( $\tau_{xy}$ ) as well as the auxiliary plane and its normal vector in ice flow direction ( $\tau_{zx}$ ) are shown in Fig. ?? fabric.

The recrystallisation does not conclusively provide arguments for the regular “diamond shape” within the multi-maxima pattern. One potential mechanism to be considered are localisation effects. In this specific example, two of the four maxima clearly correlate with such a simple shearing. For the other samples the attribution of particular maxima to simple shearing is not that obvious. The maximum at the horizontal margin ( $\tau_{zx}$ ) would vanish over time as the crystals tend to rotate towards the maximum perpendicular to the actual shear plane (Duval, 1981; Llorens et al., 2016; Journaux et al., 2019) and emphasise the vertical maximum ( $\tau_{xz}$  theory, the polycrystalline system distributes the impact of the different strain along localisation bands, especially in presence of additional aggregates such as air bubbles (Steinbach et al., 2016). This may lead to a highly variable rate of fabric change. A detailed investigation of localisation bands is rather difficult in presence of grain boundary migration (i.e. SIBM-O and SIBM-N) as recrystallisation restores the crystal shape and removes the typical shear bands (Llorens et al., 2016). Llorens et al. (2017) investigated the COF for simple shear experiments by considering localisation bands and dynamic recrystallisation (rotational recrystallisation and grain boundary migration, but without nucleation). The fact that both maxima ( $\tau_{xz}$  and  $\tau_{zx}$ ) are still visible, fits again to the assumption of a continuous recrystallisation process and relatively young but fast growing ice grains. The grain growth and especially the coarse-grained ice that can be observed in all samples in any depth are clearly a result of higher the recrystallisation component within the model, the larger the offset of the c-axis clusters from the horizontal (xy) plane of shear stress leading to two maxima on opposite sides of the high temperatures and has been observed in ice cores in Antarctica (Byrd (Gow and Williamson, 1976), Cape Folger (Thwaites et al., 1984)) as well as Greenland (GRIP (Thorsteinsson et al., 1997), NEEM (Montagnat et al., 2014)) and in several temperate glaciers (Kamb, 1959; Rigsby, 1960; Hooke and Hudleston, 1980). The largest difference though is most likely the different time horizon for the grain growth, especially compared to the polar cores pole of shear strain. According to Llorens et al. (2016), the observed multi-maxima patterns in polar cores cannot be modelled yet, as nucleation during grain boundary migration has not been implemented in the current modelling codes. However, we assume that SIBM-N is the most important process in our samples. Nevertheless, these strain-induced localisation effects might be worth to be considered for explaining multi-maxima patterns. However, there exist alternative explanations. Further alternative explanations can and should be considered: Kamb (1959) calculated the preferred maximum positions of a “diamond shape” pattern with considerations of single crystal compliance constants under recrystallisation. This explanation could add missing details to our interpretation and describe the regularity in the “diamond shape” pattern. Matsuda and Wakahama (1978) suggest twinning effects that may occur when c-axes develop under recrystallisation. Potentially, these effects may lead to a clustering of the c-axes and would even better explain the regular shape of the COF. This theory is supported by the fact that the opening angles of two opposing clusters are generally similar,

whereas the angles compared to the other two maxima can vary within 15-20° and therefore called “diamond-shape” fabrics. Apart from that, it is hard to find any studies about observations on twinning as result of ice deformation in glaciers and Faria et al. (2014b) summarised that mechanical twinning has not been observed in glacier ice yet. To investigate this further, we would need to measure the orientation of the ice crystals a-axes (in addition to the c-axes), for an enhanced image about the crystal orientation in three dimensions (Weikusat et al., 2011a; Journaux et al., 2019; Monz et al., 2020).

## 8 Conclusions

COF analyses of an ice core, extracted from a temperate alpine glacier, showed conspicuous multi-maximum multi-maxima patterns of the c-axes. This was observed at different depth levels. Generally, the azimuths of the c-axes point in the direction of the glacier flow, which coincides at the test site with the maximum compressive horizontal. The azimuth and colatitude of the centroid of these multi-maxima patterns are well-aligned with the main principal stress direction. At Close to the surface, compressional longitudinal stress conditions lead to a horizontal orientation aligned with the e-axes are thus predominantly horizontal, but with increasing depths, their colatitudes decrease. Ice flow modelling results support the assumption that this is an effect of combined compressive horizontal stresses in ice flow direction and depths increasing vertical stresses caused by the ice overburden. The presence of multi-maxima patterns (instead of a single maximum) can be explained by (i) migration recrystallisation and (ii) the presence of shear stresses. The multi-maximum patterns are also indicative that a fast and complete migration recrystallisation must have occurred. This interpretation is supported by air bubble analyses in LASM images glacier flow. In deeper parts, the dominating longitudinal shear stress causes a vertical COF. The mean basal plane is aligned with the shear plane.

Strain-induced boundary migration with nucleation of new grains (SIBM-N) seems to be the dominating recrystallisation process under the given high temperatures and strain rates. This provides an explanation for the large and branched grains accompanied by smaller grains with similar orientation and thus a clustering in several maxima. However, the observations cannot conclusively provide an answer for the characteristic “diamond-shape” pattern.

To the best of our knowledge, this is the first comprehensive COF analysis of an ice core from a temperate alpine glacier that links the COF with the glacier flow. The results are consistent with supporting measurements and modelling results. These consistencies are encouraging, and will hopefully motivate similar studies on other temperate glaciers.

*Data availability.* The ice fabric data are published in the open-access database PANGAEA® (Hellmann et al., 2018) and are available upon request. <https://doi.pangaea.de/10.1594/PANGAEA.888518>

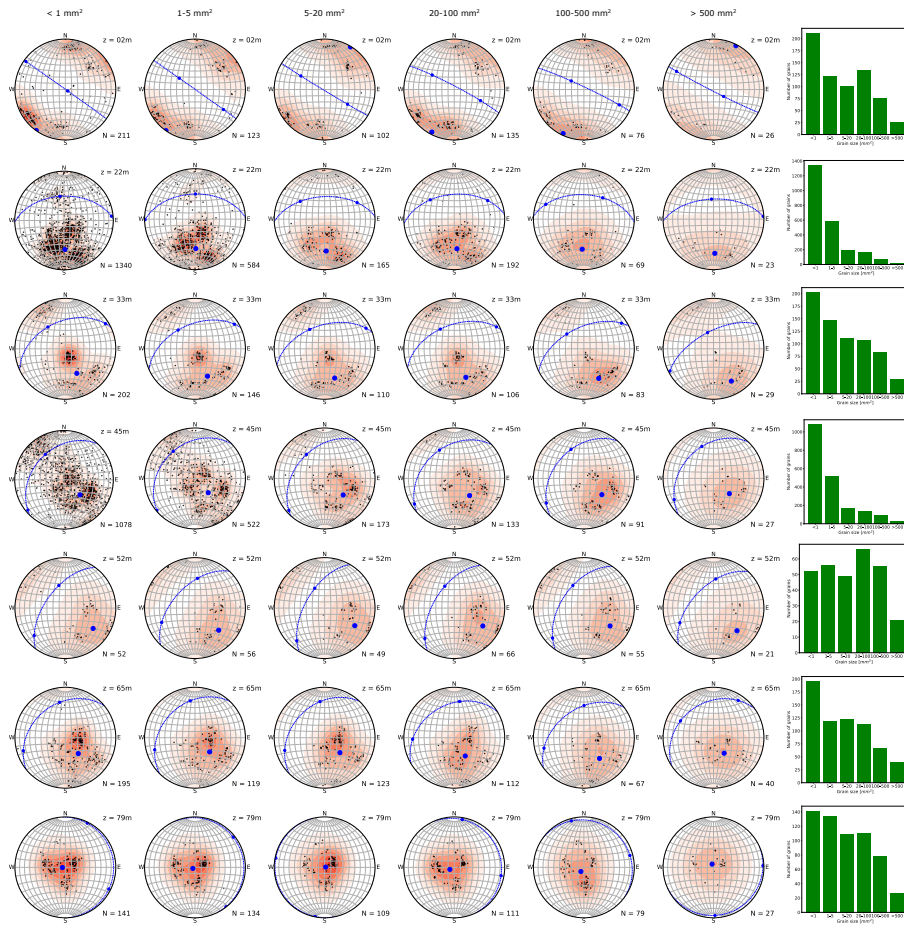


**Figure A1.** Stereo plots (lower hemisphere Schmidt equal-area projection) with the colour coded (same as Fig. 5). Each column represents a grain size class as indicated at the top. Each line represents one of the 7 samples of Fig. 5. The number of grains per class is specified for each plot. The calculated largest eigenvector for the c-axis distribution is shown as blue dot (its normal plane as dashed blue line). Last column: histograms showing the number of grains per class for each sample.

## Appendix A

*Author contributions.* This study was initiated and supervised by HM, AB, IW and MS. The field and laboratory data were collected by MS, 510 SH, MG, AB and JK and analysed by SH with support from JK and under supervision of IW and MS. Data processing and calculations were made and interpreted by SH and discussed with JK, IW, and MG. The ice flow was modelled by GJ with input data from MG. The paper was written by SH with comments and suggestions for improvements from all co-authors.

*Competing interests.* The authors declare that they have no conflict of interest.

*Acknowledgements.* This project is funded by the Swiss National Science Foundation under the SNF Grant 200021\_169329/1. Data acquisition has been provided by the Paul-Scherrer Institute, Villingen, the Alfred Wegener Institute Helmholtz Centre for Polar and Marine Research (AWI), Bremerhaven and the Laboratory of Hydraulics, Hydrology and Glaciology (VAW) of ETH Zurich. We especially thank J. Eichler, T. Gerber, T. Jenk, and D. Stampfli for their extensive technical and logistical support during ice core drilling and processing. Valuable discussions with the Structural Glaciology group at University of Tuebingen helped to improve the paper. We would like to thank the editor, Olivier Gagliardini, and the two reviewers, Erin Pettit and Peter Hudleston, for their constructive comments, which greatly improved the quality of the manuscript. 520

## References

- Alley, R. B.: Fabrics in Polar Ice Sheets: Development and Prediction, *Science*, 240, 493–495, 1988.
- Alley, R. B.: Flow-Law Hypotheses for Ice-Sheet Modeling, *Journal of Glaciology*, 38, 245–256, 1992.
- Alley, R. B., Perepezko, J. H., and Bentley, C. R.: Grain Growth in Polar Ice: I. Theory, *Journal of Glaciology*, 32, 415–424,  
525 <https://doi.org/10.3189/S0022143000012120>, 1986.
- Alley, R. B., Gow, A. J., and Meese, D. A.: Mapping C-Axis Fabrics to Study Physical Processes in Ice, *Journal of Glaciology*, 41, 197–203,  
1995.
- Alley, R. B., Gow, A. J., Meese, D. A., Fitzpatrick, J. J., Waddington, E. D., and Bolzan, J. F.: Grain-Scale Processes, Folding,  
and Stratigraphic Disturbance in the GISP2 Ice Core, *Journal of Geophysical Research: Oceans*, 102, 26 819–26 830,  
530 <https://doi.org/10.1029/96JC03836>, 1997.
- Azuma, N.: A Flow Law for Anisotropic Ice and Its Application to Ice Sheets, *Earth and Planetary Science Letters*, 128, 601–614,  
[https://doi.org/10.1016/0012-821X\(94\)90173-2](https://doi.org/10.1016/0012-821X(94)90173-2), 1994.
- Azuma, N. and Higashi, A.: Mechanical Properties of Dye 3 Greenland Deep Ice Cores, *Annals of glaciology*, 5, 1–8, 1984.
- Azuma, N., Miyakoshi, T., Yokoyama, S., and Takata, M.: Impeding Effect of Air Bubbles on Normal Grain Growth of Ice, *Journal of*  
535 *Structural Geology*, 42, 184–193, <https://doi.org/10.1016/j.jsg.2012.05.005>, 2012.
- Bauder, A., ed.: The Swiss Glaciers 2015/16 and 2016/17, vol. 137/138 of *Glaciological Report*, Cryospheric Commission (EKK) of the  
Swiss Academy of Sciences (SCNAT), [https://doi.org/10.18752/glrep\\_137-138](https://doi.org/10.18752/glrep_137-138), 2018.
- Binder, T., Garbe, C. S., Wagenbach, D., Freitag, J., and Kipfstuhl, S.: Extraction and Parametrization of Grain Boundary Networks in Glacier  
Ice, Using a Dedicated Method of Automatic Image Analysis, *Journal of Microscopy*, 250, 130–141, <https://doi.org/10.1111/jmi.12029>,  
540 2013.
- Budd, W. F.: The Development of Crystal Orientation Fabrics in Moving Ice, *Z. Gletscherkd. Glazialgeol*, 8, 65–105, 1972.
- Budd, W. F. and Jacka, T. H.: A Review of Ice Rheology for Ice Sheet Modelling, *Cold Regions Science and Technology*, 16, 107–144,  
[https://doi.org/10.1016/0165-232X\(89\)90014-1](https://doi.org/10.1016/0165-232X(89)90014-1), 1989.
- Budd, W. F., Warner, R. C., Jacka, T. H., Li, J., and Treverrow, A.: Ice Flow Relations for Stress and Strain-Rate Components from Combined  
545 Shear and Compression Laboratory Experiments, *Journal of Glaciology*, 59, 374–392, <https://doi.org/10.3189/2013JoG12J106>, 2013.
- Church, G. J., Bauder, A., Grab, M., Hellmann, S., and Maurer, H.: High-Resolution Helicopter-Borne Ground Penetrating Radar Survey to  
Determine Glacier Base Topography and the Outlook of a Proglacial Lake, in: 2018 17th International Conference on Ground Penetrating  
Radar (GPR), pp. 1–4, IEEE, Rapperswil, <https://doi.org/10.1109/ICGPR.2018.8441598>, 2018.
- Compagno, L., Jouvét, G., Bauder, A., Funk, M., Church, G., Leinss, S., and Lüthi, M. P.: Modeling the Re-Appearance of a Crashed Airplane  
550 on Gauligletscher, Switzerland, *Frontiers in Earth Science*, 7, <https://doi.org/10.3389/feart.2019.00170>, 2019.
- Cuffey, K. M. and Paterson, W. S. B.: *The Physics of Glaciers*, Elsevier, Amsterdam, fourth edn., 2010.
- Diez, A. and Eisen, O.: Seismic Wave Propagation in Anisotropic Ice – Part 1: Elasticity Tensor and Derived Quantities from Ice-Core  
Properties, *The Cryosphere*, 9, 367–384, <https://doi.org/10.5194/tc-9-367-2015>, 2015.
- Duval, P.: Creep and Recrystallization of Polycrystalline Ice, *Bulletin de Minéralogie*, 102, 80–85, <https://doi.org/10.3406/bulmi.1979.7258>,  
555 1979.
- Duval, P.: Creep and Fabrics of Polycrystalline Ice Under Shear and Compression, *Journal of Glaciology*, 27, 129–140,  
<https://doi.org/10.3189/S002214300001128X>, 1981.

- Duval, P. and Castelnau, O.: Dynamic Recrystallization of Ice in Polar Ice Sheets, *Le Journal de Physique IV*, 5, C3–197, 1995.
- Eichler, J.: C-Axis Analysis of the NEEM Ice Core—An Approach Based on Digital Image Processing, Diploma Thesis, Freie Universität Berlin, 2013.
- 560 Faria, S. H., Freitag, J., and Kipfstuhl, S.: Polar Ice Structure and the Integrity of Ice-Core Paleoclimate Records, *Quaternary Science Reviews*, 29, 338–351, <https://doi.org/10.1016/j.quascirev.2009.10.016>, 2010.
- Faria, S. H., Weikusat, I., and Azuma, N.: The Microstructure of Polar Ice. Part I: Highlights from Ice Core Research, *Journal of Structural Geology*, 61, 2–20, <https://doi.org/10.1016/j.jsg.2013.09.010>, 2014a.
- 565 Faria, S. H., Weikusat, I., and Azuma, N.: The Microstructure of Polar Ice. Part II: State of the Art, *Journal of Structural Geology*, 61, 21–49, <https://doi.org/10.1016/j.jsg.2013.11.003>, 2014b.
- Farinotti, D., Huss, M., Bauder, A., Funk, M., and Truffer, M.: A Method to Estimate the Ice Volume and Ice-Thickness Distribution of Alpine Glaciers, *Journal of Glaciology*, 55, 422–430, 2009.
- Gagliardini, O., Zwinger, T., Gillet-Chaulet, F., Durand, G., Favier, L., de Fleurian, B., Greve, R., Malinen, M., Martín, C., Råback, P.,
- 570 Ruokolainen, J., Sacchetti, M., Schäfer, M., Seddik, H., and Thies, J.: Capabilities and Performance of Elmer/Ice, a New-Generation Ice Sheet Model, *Geoscientific Model Development*, 6, 1299–1318, <https://doi.org/10.5194/gmd-6-1299-2013>, 2013.
- GlaThiDa Consortium: Glacier Thickness Database 3.0.1. World Glacier Monitoring Service, Zurich, Switzerland, <https://doi.org/10.5904/wgms-glathida-2019-03>, 2019.
- Glen, J. W.: The Creep of Polycrystalline Ice, *Proc. R. Soc. Lond. A*, 228, 519–538, <https://doi.org/10.1098/rspa.1955.0066>, 1955.
- 575 Gow, A. J. and Meese, D.: Physical Properties, Crystalline Textures and c-Axis Fabrics of the Siple Dome (Antarctica) Ice Core, *Journal of Glaciology*, 53, 573–584, <https://doi.org/10.3189/002214307784409252>, 2007.
- Gow, A. J. and Williamson, T.: Rheological Implications of the Internal Structure and Crystal Fabrics of the West Antarctic Ice Sheet as Revealed by Deep Core Drilling at Byrd Station, *Geological Society of America Bulletin*, 87, 1665–1677, 1976.
- Grab, M., Bauder, A., Ammann, F., Langhammer, L., Hellmann, S., Church, G. J., Schmid, L., Rabenstein, L., and Maurer, H. R.: Ice Volume
- 580 Estimates of Swiss Glaciers Using Helicopter-Borne GPR — an Example from the Glacier de La Plaine Morte, in: 2018 17th International Conference on Ground Penetrating Radar (GPR), pp. 1–4, <https://doi.org/10.1109/ICGPR.2018.8441613>, 2018.
- Gräff, D., Walter, F., and Bauder, A.: Borehole Measurements and Basal Velocity of Rhonegletscher: Analysis of Borehole Measurements and Determination of the Basal Sliding Velocity of Rhonegletscher, in: 15th Swiss Geoscience Meeting (SGM 2017), p. P 9.10, ETH Zurich, Laboratory for Hydraulics, Hydrology and Glaciology, <https://doi.org/10.3929/ethz-b-000444720>, 2017.
- 585 Hambrey, M. J. and Milnes, A. G.: Structural Geology of an Alpine Glacier (Griesgletscher, Valais, Switzerland), *Eclogae Geologicae Helvetiae*, 70, 667–684, 1977.
- Hambrey, M. J., Milnes, A. G., and Siegenthaler, H.: Dynamics and Structure of Griesgletscher, Switzerland, *Journal of Glaciology*, 25, 215–228, <https://doi.org/10.3189/S0022143000010455>, 1980.
- Hellmann, S., Kerch, J., Eichler, J., Jansen, D., Weikusat, I., Schwikowski, M., Bauder, A., and Maurer, H.: Crystal C-Axes
- 590 Measurements (Fabric Analyser G50) of Ice Core Samples Collected from the Temperate Alpine Ice Core Rhone\_2017, <https://doi.org/10.1594/PANGAEA.888518>, 2018.
- Herron, S. L. and Langway, C. C.: A Comparison of Ice Fabrics and Textures at Camp Century, Greenland and Byrd Station, Antarctica, *Annals of glaciology*, 3, 118–124, 1982.
- Hooke, R. L.: Crystal Shape in Polar Glaciers and the Philosophy of Ice-Fabric Diagrams, *Journal of Glaciology*, 8, 324–326,
- 595 <https://doi.org/10.3189/S002214300003135X>, 1969.

- Hooke, R. L.: Structure and Flow in the Margin of the Barnes Ice Cap, Baffin Island, N.W.T., Canada, *Journal of Glaciology*, 12, 423–438, <https://doi.org/10.3189/S0022143000031841>, 1973.
- Hooke, R. L. and Hudleston, P. J.: Origin of Foliation in Glaciers, *Journal of Glaciology*, 20, 285–299, <https://doi.org/10.3189/S0022143000013848>, 1978.
- 600 Hooke, R. L. and Hudleston, P. J.: Ice Fabrics in a Vertical Flow Plane, Barnes Ice Cap, Canada, *Journal of Glaciology*, 25, 195–214, <https://doi.org/10.3189/S0022143000010443>, 1980.
- Jacka, T. H. and Jun, L.: The Steady-State Crystal Size of Deforming Ice, *Annals of Glaciology*, 20, 13–18, <https://doi.org/10.3189/1994AoG20-1-13-18>, 1994.
- Jacka, T. H. and Maccagnan, M.: Ice Crystallographic and Strain Rate Changes with Strain in Compression and Extension, *Cold Regions Science and Technology*, 8, 269–286, [https://doi.org/10.1016/0165-232X\(84\)90058-2](https://doi.org/10.1016/0165-232X(84)90058-2), 1984.
- 605 Jansen, D., Llorens Verde, M. G., Westhoff, J., Steinbach, F., Kipfstuhl, S., Bons, P. D., Grier, A., and Weikusat, I.: Small-Scale Disturbances in the Stratigraphy of the NEEM Ice Core: Observations and Numerical Model Simulations, *The Cryosphere*, 10, 359–370, <https://doi.org/10.5194/tc-10-359-2016> <<https://doi.org/10.5194/tc-10-359-2016>> , hdl:10013/epic.46883, 2016.
- Journaux, B., Chauve, T., Montagnat, M., Tommasi, A., Barou, F., Mainprice, D., and Gest, L.: Recrystallization Processes, Microstructure and Crystallographic Preferred Orientation Evolution in Polycrystalline Ice during High-Temperature Simple Shear, *The Cryosphere*, 13, 1495–1511, <https://doi.org/10.5194/tc-13-1495-2019>, 2019.
- 610 Juvet, G. and Funk, M.: Modelling the Trajectory of the Corpses of Mountaineers Who Disappeared in 1926 on Aletschgletscher, Switzerland, *Journal of Glaciology*, 60, 255–261, <https://doi.org/10.3189/2014JoG13J156>, 2014.
- Juvet, G., Huss, M., Funk, M., and Blatter, H.: Modelling the Retreat of Grosser Aletschgletscher, Switzerland, in a Changing Climate, *Journal of Glaciology*, 57, 1033–1045, <https://doi.org/10.3189/002214311798843359>, 2011.
- 615 Kamb, B.: Experimental Recrystallization of Ice under Stress, Washington DC American Geophysical Union Geophysical Monograph Series, 16, 211, <https://doi.org/10.1029/GM016p0211>, 1972.
- Kamb, W. B.: Ice Petrofabric Observations from Blue Glacier, Washington, in Relation to Theory and Experiment, *Journal of Geophysical Research*, 64, 1891–1909, <https://doi.org/10.1029/JZ064i011p01891>, 1959.
- 620 Krischke, A., Oechsner, U., and Kipfstuhl, S.: Rapid Microstructure Analysis of Polar Ice Cores, *Optik & Photonik*, 10, 32–35, <https://doi.org/10.1002/opph.201500016>, 2015.
- Kuiper, E.-J. N., de Bresser, J. H. P., Drury, M. R., Eichler, J., Pennock, G. M., and Weikusat, I.: Using a Composite Flow Law to Model Deformation in the NEEM Deep Ice Core, Greenland: Part 2 the Role of Grain Size and Premelting on Ice Deformation at High Homologous Temperature, *The Cryosphere Discussions*, pp. 1–30, <https://doi.org/10.5194/tc-2018-275>, 2019.
- 625 Lipenkov, V. Y., Barkov, N. I., Duval, P., and Pimienta, P.: Crystalline Texture of the 2083 m Ice Core at Vostok Station, Antarctica, *Journal of Glaciology*, 35, 392–398, <https://doi.org/10.3189/S0022143000009321>, 1989.
- Llorens, M.-G., Grier, A., Bons, P. D., Lebensohn, R. A., Evans, L. A., Jansen, D., and Weikusat, I.: Full-Field Predictions of Ice Dynamic Recrystallisation under Simple Shear Conditions, *Earth and Planetary Science Letters*, 450, 233–242, <https://doi.org/10.1016/j.epsl.2016.06.045>, 2016.
- 630 Llorens, M.-G., Grier, A., Steinbach, F., Bons, P. D., Gomez-Rivas, E., Jansen, D., Roessiger, J., Lebensohn, R. A., and Weikusat, I.: Dynamic Recrystallization during Deformation of Polycrystalline Ice: Insights from Numerical Simulations, *Philosophical Transactions of the Royal Society A: Mathematical, Physical and Engineering Sciences*, 375, 20150346, <https://doi.org/10.1098/rsta.2015.0346>, 2017.

- Maohuan, H., Ohtomo, M., and Wakahama, G.: Transition in Preferred Orientation of Polycrystalline Ice from Repeated Recrystallization, *Annals of Glaciology*, 6, 263–264, <https://doi.org/10.3189/1985AoG6-1-263-264>, 1985.
- 635 Matsuda, M. and Wakahama, G.: Crystallographic Structure of Polycrystalline Ice, *Journal of Glaciology*, 21, 607–620, <https://doi.org/10.3189/S0022143000033724>, 1978.
- Montagnat, M., Azuma, N., Dahl-Jensen, D., Eichler, J., Fujita, S., Gillet-Chaulet, F., Kipfstuhl, S., Samyn, D., Svensson, A., and Weikusat, I.: Fabric along the NEEM Ice Core, Greenland, and Its Comparison with GRIP and NGRIP Ice Cores, *The Cryosphere*, 8, 1129–1138, <https://doi.org/10.5194/tc-8-1129-2014>, 2014.
- 640 Monz, M. E., Hudleston, P. J., Prior, D. J., Michels, Z., Fan, S., Negrini, M., Langhorne, P. J., and Qi, C.: Electron Backscatter Diffraction (EBSD) Based Determination of Crystallographic Preferred Orientation (CPO) in Warm, Coarse-Grained Ice: A Case Study, Storglaciären, Sweden, *The Cryosphere Discussions*, pp. 1–24, <https://doi.org/10.5194/tc-2020-135>, 2020.
- Patrick, B. A., Corvino, A. F., and Wilson, C. J. L.: Ice-Flow Measurements and Deformation at Marginal Shear Zones on Sørdsdal Glacier, Ingrid Christensen Coast, East Antarctica, *Annals of Glaciology*, 37, 60–68, <https://doi.org/10.3189/172756403781815933>, 2003.
- 645 Peternell, M., Kohlmann, F., Wilson, C. J., Seiler, C., and Gleadow, A. J.: A New Approach to Crystallographic Orientation Measurement for Apatite Fission Track Analysis: Effects of Crystal Morphology and Implications for Automation, *Chemical Geology*, 265, 527–539, <https://doi.org/10.1016/j.chemgeo.2009.05.021>, 2009.
- Petit, J. R., Jouzel, J., Raynaud, D., Barkov, N. I., Barnola, J.-M., Basile, I., Bender, M., Chappellaz, J., Davis, M., Delaygue, G., Delmotte, M., Kotlyakov, V. M., Legrand, M., Lipenkov, V. Y., Lorius, C., Pépin, L., Ritz, C., Saltzman, E., and Stievenard, M.: Climate and  
650 Atmospheric History of the Past 420,000 Years from the Vostok Ice Core, Antarctica, *Nature*, 399, 429–436, <https://doi.org/10.1038/20859>, 1999.
- Qi, C., Prior, D. J., Craw, L., Fan, S., Llorens, M.-G., Griera, A., Negrini, M., Bons, P. D., and Goldsby, D. L.: Crystallographic Preferred Orientations of Ice Deformed in Direct-Shear Experiments at Low Temperatures, *The Cryosphere*, 13, 351–371, 2019.
- Rigsby, G. P.: Crystal Fabric Studies on Emmons Glacier Mount Rainier, Washington, *The Journal of Geology*, 59, 590–598, 1951.
- 655 Rigsby, G. P.: Crystal Orientation in Glacier and in Experimentally Deformed Ice, *Journal of Glaciology*, 3, 589–606, 1960.
- Robin, G. D. Q., Mitchell, G. F., and West, R. G.: Ice Cores and Climatic Change, *Philosophical Transactions of the Royal Society of London. B, Biological Sciences*, 280, 143–168, <https://doi.org/10.1098/rstb.1977.0103>, 1977.
- Russell-Head, D. S. and Budd, W. F.: Ice-Sheet Flow Properties Derived from Bore-Hole Shear Measurements Combined With Ice-Core Studies, *Journal of Glaciology*, 24, 117–130, <https://doi.org/10.3189/S0022143000014684>, 1979.
- 660 Schulson, E. M. and Duval, P.: Creep and Fracture of Ice, 2009.
- Schwikowski, M., Jenk, T. M., Stampfli, D., and Stampfli, F.: A New Thermal Drilling System for High-Altitude or Temperate Glaciers, *Annals of Glaciology*, 55, 131–136, <https://doi.org/10.3189/2014AoG68A024>, 2014.
- Steinbach, F., Bons, P. D., Griera, A., Jansen, D., Llorens Verde, M. G., Roessiger, J., and Weikusat, I.: Strain Localization and Dynamic Recrystallization in the Ice–Air Aggregate: A Numerical Study, *The Cryosphere*, 10, 3071–3089, <https://doi.org/10.5194/tc-10-3071-2016>,  
665 2016.
- Steinbach, F., Kuiper, E.-J. N., Eichler, J., Bons, P. D., Drury, M. R., Griera, A., Pennock, G. M., and Weikusat, I.: The Relevance of Grain Dissection for Grain Size Reduction in Polar Ice: Insights from Numerical Models and Ice Core Microstructure Analysis, *Frontiers in Earth Science*, 5, <https://doi.org/10.3389/feart.2017.00066>, 2017.

- Thompson, L. G., Mosley-Thompson, E., Davis, M. E., Henderson, K. A., Brecher, H. H., Zagorodnov, V. S., Mashiotta, T. A., Lin, P.-N.,  
670 Mikhalenko, V. N., Hardy, D. R., and Beer, J.: Kilimanjaro Ice Core Records: Evidence of Holocene Climate Change in Tropical Africa,  
*Science*, 298, 589–593, <https://doi.org/10.1126/science.1073198>, 2002.
- Thorsteinsson, T., Kipfstuhl, J., and Miller, H.: Textures and Fabrics in the GRIP Ice Core, *Journal of Geophysical Research: Oceans*, 102,  
26 583–26 599, <https://doi.org/10.1029/97JC00161>, 1997.
- Thwaites, R. J., Wilson, C. J. L., and McCray, A. P.: Relationship Between Bore-Hole Closure and Crystal Fabrics in Antarctic Ice Core from  
675 Cape Folger, *Journal of Glaciology*, 30, 171–179, <https://doi.org/10.3189/S0022143000005906>, 1984.
- Tison, J.-L. and Hubbard, B.: Ice Crystallographic Evolution at a Temperate Glacier: Glacier de Tsanfleuron, Switzerland, Geological Society,  
London, Special Publications, 176, 23–38, 2000.
- Vollmer, F. W.: C Program for Automatic Contouring of Spherical Orientation Data Using a Modified Kamb Method, *Computers & Geo-*  
*sciences*, 21, 31–49, 1995.
- 680 Wallbrecher, E.: Tektonische Und Gefügeanalytische Arbeitsweisen: Graphische, Rechnerische Und Statistische Verfahren, Enke, Stuttgart,  
1986.
- Weikusat, I., Kipfstuhl, S., Azuma, N., Faria, S. H., and Miyamoto, A.: Deformation Microstructures in an Antarctic Ice Core (EDML) and  
in Experimentally Deformed Artificial Ice, *Low Temperature Science*, 68, 115–123, 2009a.
- Weikusat, I., Kipfstuhl, S., Faria, S. H., Azuma, N., and Miyamoto, A.: Subgrain Boundaries and Related Microstructural Features in EDML  
685 (Antarctica) Deep Ice Core, *Journal of Glaciology*, 55, 461–472, <https://doi.org/10.3189/002214309788816614>, 2009b.
- Weikusat, I., De Winter, D. A. M., Pennock, G. M., Hayles, M., Schneijdenberg, C., and Drury, M. R.: Cryogenic EBSD on Ice: Preserving  
a Stable Surface in a Low Pressure SEM, *Journal of microscopy*, 242, 295–310, 2011a.
- Weikusat, I., Miyamoto, A., Faria, S. H., Kipfstuhl, S., Azuma, N., and Hondoh, T.: Subgrain Boundaries in Antarctic Ice Quantified by  
X-Ray Laue Diffraction, *Journal of Glaciology*, 57, 111–120, <https://doi.org/10.3189/002214311795306628>, 2011b.
- 690 Weikusat, I., Jansen, D., Binder, T., Eichler, J., Faria, S. H., Wilhelms, F., Kipfstuhl, S., Sheldon, S., Miller, H., Dahl-Jensen, D., and Kleiner,  
T.: Physical Analysis of an Antarctic Ice Core—towards an Integration of Micro- and Macrodynamics of Polar Ice, *Philosophical Trans-*  
*actions of the Royal Society A: Mathematical, Physical and Engineering Sciences*, 375, 20150 347, <https://doi.org/10.1098/rsta.2015.0347>,  
2017.
- Wilson, C. J., Russell-Head, D. S., and Sim, H. M.: The Application of an Automated Fabric Analyzer System to the Textural Evolution of  
695 Folded Ice Layers in Shear Zones, *Annals of Glaciology*, 37, 7–17, 2003.
- Wilson, C. J. L. and Peterzell, M.: Evaluating Ice Fabrics Using Fabric Analyser Techniques in Sørdsal Glacier, East Antarctica, *Journal of*  
*Glaciology*, 57, 881–894, <https://doi.org/10.3189/002214311798043744>, 2011.